ANL-8039

ANL-8039

DEVELOPMENT OF HIGH-SPECIFIC-ENERGY BATTERIES FOR ELECTRIC VEHICLES

Progress Report for the Period February 1973—July 1973

P. A. Nelson, E. C. Gay, R. K. Steunenberg,
J. E. Battles, W. W. Schertz, D. R. Vissers,
K. M. Myles, M. L. Kyle, D. S. Webster,
and L. Burris

U of C-AUA-USAEC

ARGONNE NATIONAL LABORATORY, ARGONNE, ILLINOIS

Work done for the National Science Foundation
under an Agreement between the
U.S. Atomic Energy Commission and
the National Science Foundation

DISCLAIMER

Printed in the United States of America
Available from
National Technical Information Service
U.S. Department of Commerce
5285 Port Royal Road
Springfield, Virginia 22151
Price: Printed Copy $5.45; Microfiche $1.45

ANL-8039
Chemistry

ARGONNE NATIONAL LABORATORY
9700 South Cass Avenue
Argonne, Illinois 60439

DEVELOPMENT OF HIGH-SPECIFIC-ENERGY BATTERIES FOR ELECTRIC VEHICLES

Progress Report for the Period
February 1973—July 1973

by

P. A. Nelson, E. C. Gay, R. K. Steunenberg,
J. E. Battles, W. W. Schertz, D. R. Vissers,
K. M. Myles, M. L. Kyle, D. S. Webster,
and L. Burris

Chemical Engineering Division

December 1973

Previous reports in this series

ANL-7888	December 1971
ANL-7953	September 1972
ANL-7998	April 1973

FOREWORD

This is the third semiannual technical progress report of a research and development program conducted by the Chemical Engineering Division of Argonne National Laboratory under an agreement between the United States Atomic Energy Commission and the National Science Foundation (RANN Program). The period covered by this report is February 1, 1973 through July 31, 1973.

The goal of this program is to develop, construct, and test lithium/sulfur batteries suitable for the propulsion of high-performance electric automobiles. The immediate goals include the development of reliable sealed cells appropriate for use in a 1-kW battery.

Overall program management is the responsibility of Mr. L. Burris, Division Director, and Mr. D. S. Webster, Associate Division Director. Technical direction is provided by Dr. P. A. Nelson, Section Head and Drs. R. K. Steunenberg, E. C. Gay, and J. E. Battles, Group Leaders. The National Science Foundation Representative is Dr. Leonard Topper.

TABLE OF CONTENTS

	Page
ABSTRACT	1
SUMMARY	1
I. INTRODUCTION	5
II. CELL STUDIES	7
A. Goals	7
B. Designs of Experimental Cells	7
C. Cell Operations and Results	11
1. Sulfur-10 at. % Arsenic Sulfur-Electrode Mixtures	15
2. Sulfur-40 at. % Arsenic Sulfur-Electrode Mixtures	17
3. Sulfur-23.7 at. % Arsenic Sulfur-Electrode Mixtures	25
D. Summary and Conclusions	25
III. SUPPORTING LABORATORY STUDIES	27
A. Lithium-Electrode Development Studies	27
1. Lithium-Electrode Support Materials	27
2. Lithium-Retention Studies	28
3. Post-Test Examination of Lithium Electrodes	30
B. Solubility of Lithium in Molten LiCl-KCl Electrolyte	31
C. Solid-Electrode Studies	32
IV. MATERIALS TESTING AND FABRICATION	34
A. Feedthrough Development	34
B. Insulator and Separator Studies	39
C. Materials Evaluation	41
1. Evaluation of Metals	41
2. Evaluation of Ceramics	43
REFERENCES	47

LIST OF FIGURES

No.	Title	Page
1.	Sulfur Electrode Type I	9
2.	Sulfur Electrode Type III	9
3.	Sulfur Electrode Type V	9
4.	Bicell Configuration for Lithium/Sulfur Cells	10
5.	Configuration of Welded Lithium/Sulfur Cell	10
6.	Configuration of Cell with Sulfur Electrode Type VI	11
7.	Discharged Products for Cell WS-4	16
8.	Capacity Density as a Function of Cycle Number for Cell S-35	18
9.	Capacity Density as a Function of Cycle Number for Cell S-38	20
10.	Voltage-Capacity Density Curves for Cell S-38	20
11.	Sulfur Utilization and Ampere-Hour Efficiency *vs.* Discharge Cycle Number for Cell WS-11	21
12.	Sulfur Utilization and Ampere-Hour Efficiency *vs.* Discharge Cycle Number for Cell WS-12	21
13.	Cell and Reference Voltages during Discharge as Functions of Cell Life for Cell WS-12	22
14.	Cell Voltage *vs.* Percent of Theoretical Capacity during Discharge of Cell WS-13	23
15.	Cell for Lithium-Retention Studies	29
16.	Schematic Representation of Brazed-Type Feedthrough	35
17.	Schematic Representation of Brazed-Type Feedthrough for Materials of Construction with Different Coefficients of Thermal Expansion	36
18.	Photomacrograph of Cross-Section of Brazed Feedthrough	37
19.	Photomicrograph Showing Excellent Bonding of Braze Metal to $CaZrO_3$ Insulator	37
20.	Photomacrograph of Cross-Section of Brazed Feedthrough Showing Thermal Cracks at Sleeve/Ceramic Interface	38
21.	Photomicrograph of As-Sintered $CaZrO_3$ Showing a Low-Melting Impurity Phase at Particle Boundaries	43
22.	Photomicrograph Showing Conductive Layer Formed on Surface of $CaZrO_3$ Exposed to Lithium at 400°C for 600 hr	44
23.	$CaZrO_3$ Exposed to Lithium at 400°C for 400 hr	46

LIST OF TABLES

No.	Title	Page
I.	Goals for a High-Specific-Energy Lithium/Sulfur Battery for Electric Automobiles	5
II.	Summary of Physical Characteristics and Performance Data of Li/LiF-LiCl-KCl/S-As Cells	12
III.	Current-Collector and Sheath Materials Used in Lithium/Sulfur Cells	14
IV.	Weights of Components of Welded Cell S-39	24
V.	Potential Support Materials for Lithium Electrodes	27
VI.	Distribution of Lithium after Operation of Li/LiCl-KCl/Li(Al) Cell	30
VII.	$CaZrO_3$ Pressed at 10,000 psi and Sintered at 1450°C for 60 hr.	41
VIII.	Results of Planned-Interval Corrosion Tests in LiF-LiCl-KCl Electrolyte at 400°C	42

DEVELOPMENT OF HIGH-SPECIFIC-ENERGY BATTERIES FOR ELECTRIC VEHICLES

Progress Report for the Period
February 1973—July 1973

by

P. A. Nelson, E. C. Gay, R. K. Steunenberg,
J. E. Battles, W. W. Schertz, D. R. Vissers,
K. M. Myles, M. L. Kyle, D. S. Webster,
and L. Burris

ABSTRACT

This report, which covers the period from February 1973 to July 1973, describes the research efforts on a program, sponsored by the National Science Foundation, to develop a high-specific-energy lithium/sulfur battery having the performance characteristics required for powering pollution-free automobiles. The cells currently under development have negative electrodes of molten lithium and positive electrodes of sulfur (plus an additive to reduce the sulfur vapor pressure) separated by a molten lithium halide-containing electrolyte. The operating temperature of the cells is about 400°C.

The performance goals for a single cell include a capacity density of 0.4 A-hr/cm^2 at a current density of 0.1 A/cm^2, a peak power density of 1-2 W/cm^2, and a minimum cycle life of 1000 cycles. Cells with positive electrodes consisting of sulfur-arsenic-carbon mixtures in graphite housings have achieved short-time peak power densities and capacity densities that meet or exceed the goals for a single cell. A capacity density of 0.1 A-hr/cm^2 has been sustained at a discharge current density of 0.1 A/cm^2 (1-V cutoff) for more than 500 hr and 100 cycles. Improvement in cell design is needed, however, to achieve higher sulfur utilization and longer cell lifetimes.

The cell development program is supported by (1) laboratory studies to investigate chemical reactions occurring in the cells and (2) materials studies to identify materials of construction that are compatible with the cell environment and to design and fabricate cell components.

SUMMARY

Cell Studies

The objective of the cell studies is to develop the technology required for a multikilowatt lithium/sulfur battery for use in electrically powered vehicles. The performance goals that have been established for a single

cell include a capacity density of 0.4 A-hr/cm^2 (70% of the theoretical capacity density) at a current density of 0.1 A/cm^2 to a 1.0-V cutoff (IR-included) with an average discharge voltage of 1.8 V. Effort is being directed toward development of a cell having a positive electrode of sulfur (plus an additive to lower the sulfur vapor pressure) and a negative electrode of liquid lithium contained in a porous metal; the electrodes are separated by a lithium halide-containing molten-salt electrolyte. The cell design that has tentatively been chosen is a bicell design, in which the sulfur electrode is surrounded by the lithium electrode.

A number of additives have been used in the sulfur electrodes to decrease the thermodynamic activity of the sulfur and to increase its electronic conductivity. Decreasing the activity of the sulfur may increase the lifetimes of cells by reducing the loss of sulfur through vaporization or solubility in the electrolyte. Increasing the electronic conductivity of the sulfur should result in improved cell performance. In the cells operated during this reporting period, various amounts of arsenic (10 to 40 at. %) were added to the sulfur to test the effectiveness of arsenic in reducing the rate of sulfur escape from the sulfur electrode.

Short-time peak power densities greater than the goal of 1 to 2 W/cm^2 have been achieved with positive electrodes consisting of sulfur-arsenic-carbon mixtures in graphite housings. Moreover, the sulfur utilization goal (70% of the theoretical capacity density at 0.1 A/cm^2 to a 1.0-V cutoff) has been exceeded for a few cycles. A capacity density of 0.1 A-hr/cm^2 (about 30% of the theoretical capacity density) has been sustained at a discharge current density of 0.1 A/cm^2 to a 1.0-V cutoff for an operating period of more than 500 hr and 100 cycles. This performance represents significant progress over the performance of earlier cells operated in this program.

To develop longer-lived cells with the performance required for vehicle propulsion, further effort appears to be required in the following major areas: (1) improvement of lithium containment in the current collector and (2) achievement of higher sulfur utilization (70% of the theoretical capacity density) for hundreds of hours and hundreds of cycles. Also needed for the development of long-lived cells are corrosion-resistant feedthroughs and separators. As these components are developed, their compatibility with the cell environment will be determined by long-term tests in operating cells.

Laboratory Studies

Laboratory investigations are being conducted on the lithium retention characteristics of the negative electrode of lithium/sulfur cells. These investigations include studies of various support materials for the liquid lithium, determination of the effect of moisture on the retention of lithium by the electrode, and examinations of lithium electrodes from lithium/sulfur test cells. Steel wool and expanded mild steel mesh appear promising as low-cost, light-weight support materials. Cycling tests in which lithium was transferred electrochemically between a steel wool electrode and a lithium-aluminum alloy counterelectrode indicated good retention of the liquid lithium by the steel wool. Preliminary results indicated that small amounts of moisture (10-25 ppm) added to the electrolyte by introducing water vapor into the system had little or no effect on lithium retention. Larger amounts (>150 ppm), however, did interfere with the lithium retention characteristics

of the electrode during the complete charge and discharge cycling of the cell. Analytical studies that were performed on two nickel Feltmetal electrodes from lithium/sulfur cell tests showed the presence of sulfide in a lithium electrode that had performed poorly and its absence in one that had performed well.

A survey of the literature has indicated that the solubility of lithium metal in molten LiCl-KCl eutectic at 400°C is about 0.13 mol %. Assuming a diffusion coefficient of 10^{-5} cm^2 sec^{-1}, complete self-discharge of a lithium/sulfur cell through diffusion of lithium to the sulfur electrode is estimated to require about 270 days.

Ceramic electrolyte materials such as beta alumina ($Na_2O \cdot 11Al_2O_3$) are used in sodium/sulfur batteries. A brief study was initiated to investigate the possibility of using the lithium analog of sodium beta alumina in lithium/sulfur cells. A commercially produced beta-alumina tube was treated successfully with molten $AgNO_3$ to replace the sodium ions with silver ions. However, when an attempt was made to substitute lithium ions for the silver ions by an electrochemical procedure, the solid electrolyte was severely fractured. No further work on solid electrolytes is planned for the near future.

Materials Testing and Fabrication

The development efforts of the materials program involve the evaluation and selection of corrosion-resistant materials (metallic and ceramic), and the design, development, and fabrication of various cell components, such as electrical feedthroughs, cell housings, current collectors, insulators, and separators.

Development of a brazed feedthrough has proceeded to the point where operative feedthroughs have been supplied to the cell development group for in-cell testing and evaluation. Several problem areas remain before hermetically tight seals can be routinely produced. Solutions to these problems have been considered, but large investments of programmatic effort will be deferred until the in-cell reliability of the present feedthrough design has been established.

Lithium/sulfur batteries for vehicular propulsion will require ceramic or insulator materials for several functions, *e.g.*, electrical feedthrough insulators and electrode separators. The selection of materials for potential application are limited to those that will withstand the corrosive environment of the cell. Based on preliminary lithium-compatibility test results (and other factors), calcium zirconate appeared suitable for feedthrough insulators.

Procedures have been developed for the fabrication of $CaZrO_3$ insulators, using normal pressing-and-sintering techniques, which yield a product that is 94 to 98% of theoretical density and impervious to air. Metallographic and electron microprobe examinations of sintered specimens prepared from as-received $CaZrO_3$ powder have confirmed the presence of a calcium silicate impurity phase at the particle boundaries. Also, these examinations have indicated that the sintered material contains some incompletely reacted CaO and ZrO_2. Additional lithium-compatibility tests on $CaZrO_3$ have indicated that this material is dispersed and tends to form a conductive surface layer when exposed to lithium at 400°C for 600 to 1000 hr. Although this behavior

appears to be related to impurities in the $CaZrO_3$, the specific impurities involved and the mechanism have not been identified.

Planned-interval corrosion tests in LiF-LiCl-KCl electrolyte at 400°C have been completed for a number of stainless steels and pure iron. The measured corrosion rates were very low (<10 μm/yr) for the stainless steels. High-purity iron (99.999%) was less corrosion resistant than Armco ingot iron.

A porous ceramic cloth or paper which is resistant to the cell environment (particularly lithium) is a desirable material for electrode separators. Tests samples of Y_2O_3 cloth have been obtained and tested for compatibility with lithium at 400°C. All samples showed small areas of slight darkening, but there was no apparent change in the resistivity of the material. Tests of Y_2O_3 cloth in operating cells are planned.

I. INTRODUCTION

This is the third semiannual progress report on a program, sponsored by the National Science Foundation (NSF), that is directed toward the development of a high-specific-energy (>200 W-hr/kg), high-specific-power (>200 W/kg) battery suitable for powering an all-electric automobile. The overall program is expected to progress through several stages of development of successively larger batteries, terminating in a prototype battery of about 60-kW peak power, capable of storing up to about 35 kW-hr of energy. This size battery would be suitable for powering a vehicle weighing about 1300 kg. Demonstration of a full-size battery would probably be possible, with adequate funding, before the end of the decade. Development beyond this point should probably be undertaken by industry.

The immediate goal of the program is the development of a sealed lithium/sulfur cell that operates at a performance level consistent with the overall goals of the program. The performance goals for the battery and for a single cell are given in Table I. These goals are now being reassessed in relation to both near-term and long-term objectives.

TABLE I. Goals for a High-Specific-Energy Lithium/Sulfur Battery for Electric Automobiles

Assembled Battery	
Specific energy (at the 4-hr rate)	200 W-hr/kg
Specific power (at the 1-hr rate)	200 W/kg
Cost[a]	$10/kW-hr
Lifetime	3-yr minimum
Cycle life	1000 cycles
Single Cell	
Specific energy	220 W-hr/kg
Specific power	220 W/kg
Cost[a]	$9/kW-hr
Capacity density (at the 1-hr rate)	0.4 A-hr/cm^2
Sulfur utilization (above 1-V cutoff)	70%
Capacity per unit volume of sulfur electrode	1.0 A-hr/cm^3
Cycle life	1000 minimum

[a]Cost of battery capacity, not direct energy cost.

The program is subdivided into three general areas of investigation: (1) cell studies, in which experimental cells are designed, built, and operated to obtain electrical performance data, and cell components are tested under cell operating conditions, (2) supporting laboratory studies, in which specific chemical problems that arise during cell development are investigated, and (3) materials studies, in which materials of construction for cell components are evaluated and tested and cell components are designed and fabricated.

A parallel program at ANL, sponsored by the U.S. Atomic Energy Commission

(AEC), is directed toward the development of lithium/sulfur batteries for use as energy storage devices in electrical utility networks. The desired duty cycle (10- to 14-hr discharge; 6-to 8-hr charge) for off-peak energy storage batteries results in battery-performance requirements (especially in specific power) quite different from those of the automobile propulsion application. These differences in requirements lead to a natural division of effort between the two programs. However, the efforts are coordinated under a common management structure at ANL to avoid overlap or duplication. Where appropriate, the division of effort between the AEC and NSF programs is described and the expected benefits to the NSF program to be gained from the parallel effort in the AEC program are indicated.

II. CELL STUDIES
(E. C. Gay)

A. Goals

The objective of the cell studies is to develop the technology required for a multikilowatt lithium/sulfur battery for use in electrically powered vehicles.

Effort is being directed toward development of a cell having a positive electrode of sulfur (plus an additive to lower the sulfur vapor pressure) and a negative electrode of liquid lithium contained in a porous metal; the electrodes are separated by a molten-salt electrolyte. The cell design that has tentatively been chosen is a bicell design in which the sulfur electrode is surrounded by the lithium electrode. The performance goals that have been established for a single cell include a capacity density of 0.4 A-hr/cm^2 (70% of the theoretical capacity density) at a current density of 0.1 A/cm^2 to a 1-V cutoff, with an average discharge voltage of 1.8 V.

The cells presently being operated have sulfur-electrode areas of approximately 20 cm^2. When separators and feedthroughs that withstand molten lithium have been developed, cells will be scaled up to electrode areas of 60 to 250 cm^2 and will serve as components of a 1- to 2-kW battery. Interim studies of scaled-up cells may be undertaken using Li-Al solid electrodes as negative electrodes to avoid corrosion of the ceramic parts. (Development of cells having Li-Al electrodes is now receiving primary attention in the parallel program on lithium/sulfur batteries sponsored by the AEC.)

Studies of cells containing a single lithium electrode have provided an effective means of evaluating the performance of cell components, especially the electrodes. The purpose of the present cell tests has been to evaluate the electrical performance, lifetime, and cycle life of cells. Improvements in the cell performance have been sought by changing the sulfur-electrode composition, the methods of assembly for the cells, or the design of cell components. Several investigations of cells of the bicell design have also been conducted. As further progress is made with cells having a single lithium electrode, efforts to operate cells of the bicell design will be increased.

Nineteen gasketed sealed cells of approximately 20-cm^2 electrode area were operated during this reporting period. The objectives of these experiments were as follows: (1) to develop cells with graphite sulfur-electrode housings and metal lithium-electrode housings that meet the cell performance goals, (2) to evaluate the effect of the addition of various amounts of arsenic on sulfur containment, (3) to develop techniques for improving lithium containment in porous-metal structures, and (4) to evaluate the corrosion resistance of various cell components under cell operating conditions.

B. Designs of Experimental Cells
(W. W. Schertz, F. J. Martino, K. E. Anderson)

A number of cell designs have been developed and tested in the course of the cell-performance studies.[1,2] In the initial cell studies, relatively large

amounts of metal (molybdenum, niobium, tungsten) were used as sulfur-electrode current collectors, and the sulfur electrode was in contact with the cell housing. Niobium or molybdenum housings were used because static corrosion tests had indicated that these materials were resistant to attack by lithium-sulfur mixtures and electrolyte. Later experiments showed, however, that niobium and molybdenum reacted with the LiF-LiCl-KCl electrolyte at the sulfur electrode potential. In more recent cell designs, therefore, the cell housing has been in contact only with the lithium electrode, and a graphite housing has been used to contain the sulfur and to serve as a current collector. In cells containing molybdenum components at the sulfur-electrode potential, the charge cutoff voltage has been maintained below 2.7 V to avoid any reaction between molybdenum and the electrolyte.

Various additives, *e.g.*, thallium, selenium, phosphorus and arsenic, have been used in sulfur electrodes to decrease the thermodynamic activity of the sulfur and to increase its electronic conductivity.[1-3] Decreasing the activity of the sulfur may increase the lifetimes of cells by reducing the loss of sulfur through vaporization or solubility in the electrolyte. Increasing the electronic conductivity of the sulfur should result in improved cell performance. In the cells operated during this reporting period, various amounts of arsenic (10 to 40 at. %) were added to the sulfur to test the effectiveness of arsenic in reducing the rate of sulfur escape from the sulfur electrode.

The negative electrode of the cells consists of a porous metal structure, which serves as the current collector, impregnated with liquid lithium. In the present studies, different current collector materials (porous nickel, porous stainless steel, and steel wool) were used in an effort to improve lithium retention in the negative electrode.

Improvements in sulfur utilization were sought by using sulfur electrodes of different designs. The designs used are as follows:

Type I. A high-density graphite housing containing a porous graphite structure which was infiltrated with electrolyte and had 1/4-in.-dia or 1/2-in.-dia holes to hold the sulfur-electrode mixture. A porous graphite disk infiltrated with electrolyte was used as the sheath material.

Type II. A high-density graphite housing containing a powdered sulfur-arsenic mixture, carbon black, and electrolyte. Occasionally, tungsten wire or corrugated molybdenum mesh was used as a current collector. A porous graphite disk infiltrated with electrolyte was used as the sheath material.

Type III. A molybdenum foam structure infiltrated with electrolyte which served as the sulfur-electrode housing. Molybdenum foam was also used for the sheath and the current collector.

Type IV. A high-density graphite housing containing a porous graphite structure which was impregnated with the sulfur-electrode material.

Type V. A reference electrode used in conjunction with one of the above sulfur-electrode configurations.

Type VI. An open sulfur-electrode structure formed with a tungsten wire basket and zirconia cloth.

The electrode designs of Types I, III, and V are shown in Figs. 1, 2, and 3, respectively.

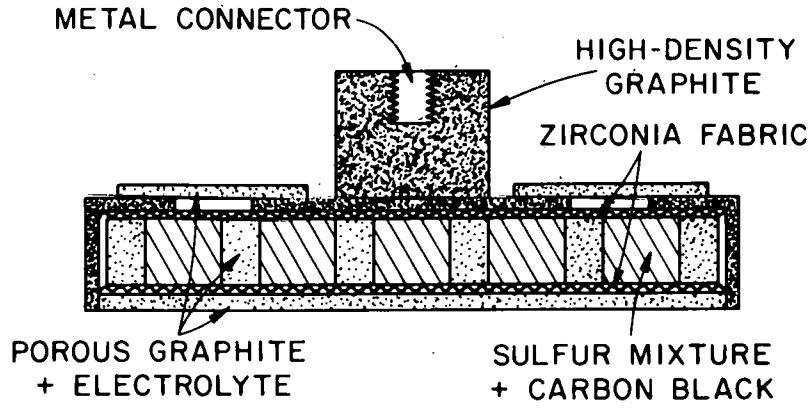

Fig. 1.

Sulfur Electrode Type I

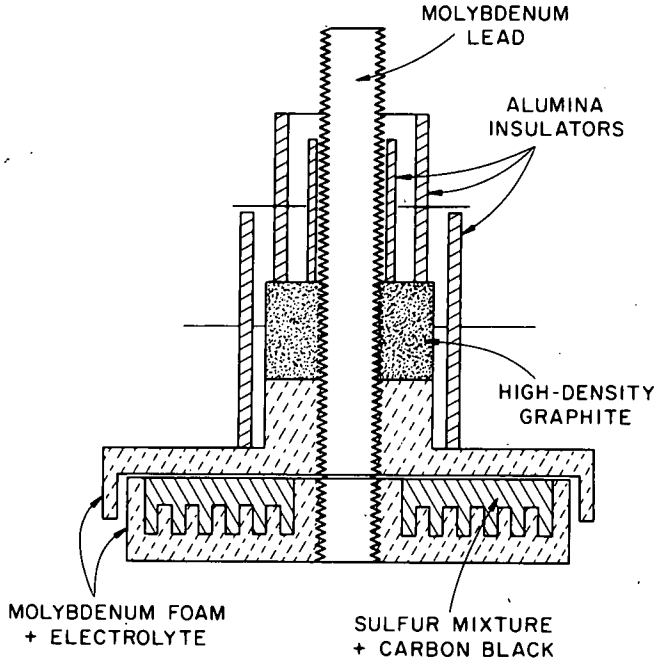

Fig. 2.

Sulfur Electrode Type III

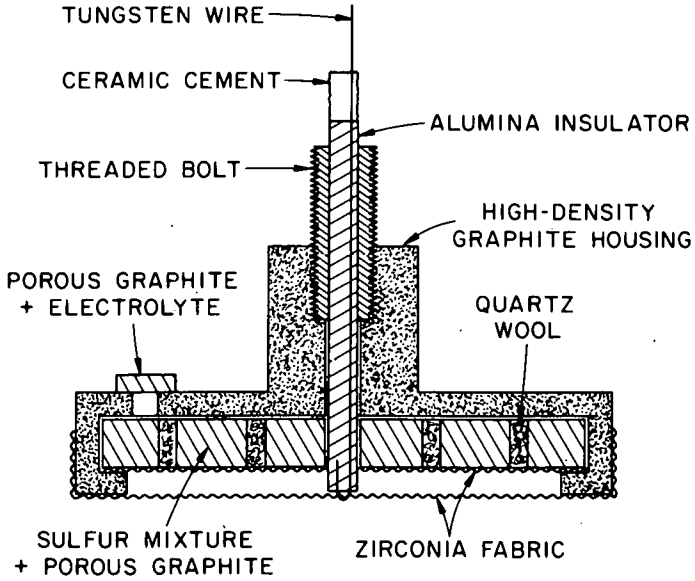

Fig. 3.

Sulfur Electrode Type V

Typical cell designs used in these investigations are shown in Figs. 4, 5, and 6. In the bicell design shown in Fig. 4, the metal housing is at the lithium electrode potential, and an insulated feedthrough is required to conduct current from the sulfur electrode. The bicell design was used in several of the cell tests; however, in most of the tests, a cell design was employed in which the upper lithium electrode was not included (in other respects, the

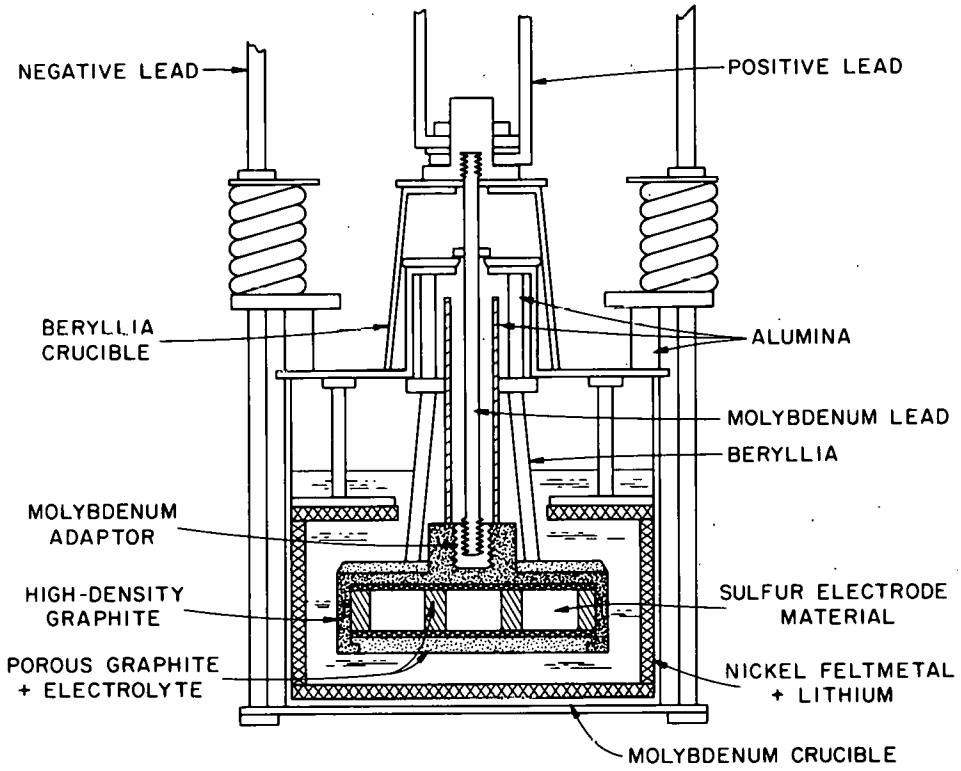

Fig. 4. Bicell Configuration for Lithium/Sulfur Cells

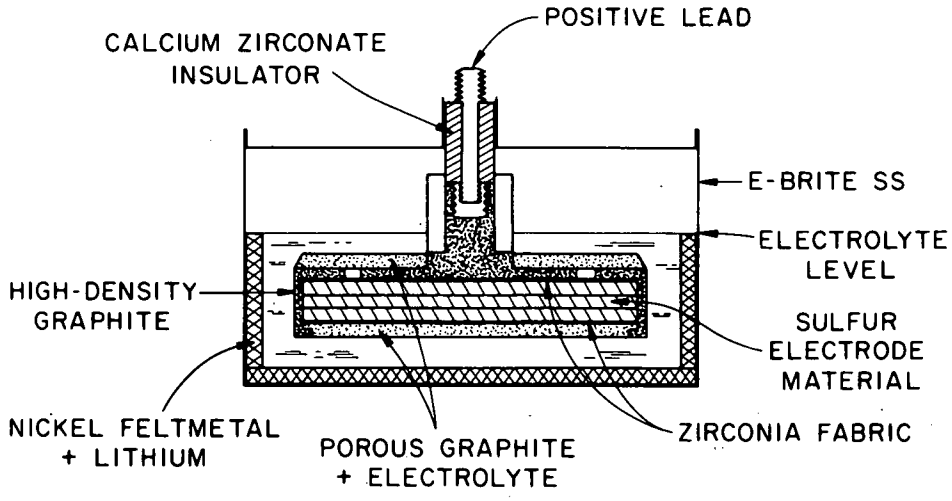

Fig. 5. Configuration of Welded Lithium/Sulfur Cell

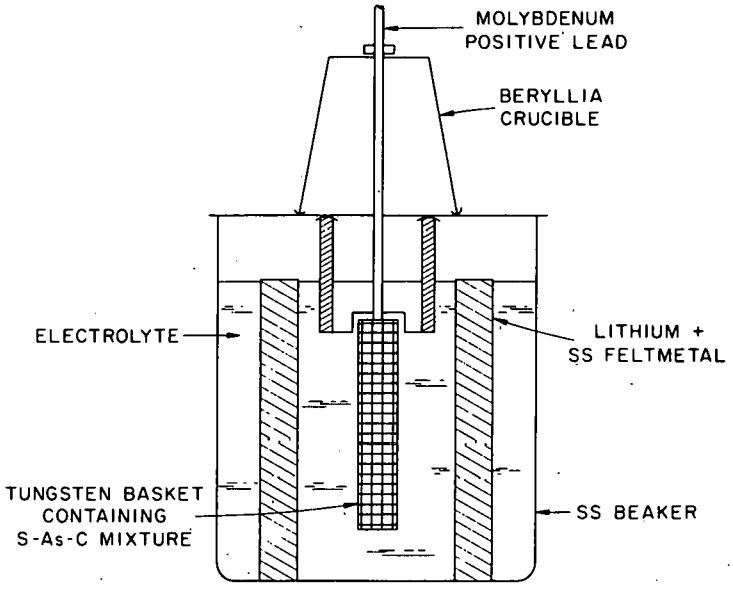

Fig. 6. Configuration of Cell with Sulfur Electrode Type VI

design was very similar to that shown in Fig. 4). As suitable feedthroughs and separators are developed, some of the components used in these cells can be eliminated and lighter weight cells with smaller interelectrode distances can be designed. The cell shown in Fig. 5 was used to test the performance of a welded cell having a feedthrough with a $CaZrO_3$ insulator. The cell configuration shown in Fig. 6 was used in an attempt to prepare a discharged sulfur electrode (Li_2S + additive + carbon black mixture) which could be degassed and used in one of the sulfur-electrode configurations described above. A sulfur electrode of Type VI was used in these experiments.

A summary of the physical and design characteristics of the cells is given in Table II. A description of the various types of current-collector and sheath materials used in the cells is given in Table III.

C. Cell Operations and Results
(W. W. Schertz, F. J. Martino, K. E. Anderson)

All cells were operated in a furnace well that was attached to the floor of a helium-atmosphere glovebox and was heated by an electric resistance furnace. The helium atmosphere generally contained less than 5 ppm (by volume) of oxygen and moisture.

The cells were discharged at constant currents with the aid of a dc power supply. Two charging techniques were used. The technique used most frequently was charging at constant current to a preset charge cutoff voltage. Alternatively, charging was accomplished by maintaining a constant voltage across the cell terminals. Constant-voltage charging is of interest because it appears that the lithium/sulfur cells can be charged much more rapidly using this technique. The cells were connected to a meter relay that automatically reversed the polarity of the power supply when the cell reached the preset cutoff voltage for

TABLE II. Summary of Physical Characteristics[a] and Performance Data of Li/LiF-LiCl-KCl/S-As Cells (all interelectrode distances = 0.6 cm).

Cell No.	S-31	S-33	S-34	WS-4	WS-5	WS-6	S-35	S-36	S-37	S-38
Lithium Electrode										
Area, cm^2	100.1	100.1	100.1	135.0	135.0	100.0	100.1	152.0	100.1	100.1
Wt. of Li, g	7.0	6.8	7.0	14.5	15.0	3.5	7.0	8.5	5.5	5.7
Current collector	Ni	Ni	Ni	SS	SS	Ni	Ni	Ni	Ni	Ni
Thickness, cm	0.2	0.2	0.2	0.6	0.6	0.2	0.2	0.2	0.2	0.2
Sulfur Electrode										
Area, cm^2 (Elect. config.)[b]	20.3(II)	20.3(II)	20.3(II)	40.6(VI)	40.6(VI)	20.3(II)	20.3(I)	27.3(I)	20.3(I)	20.3(I)
Thickness, cm	1.0	0.5	0.5	0.9	0.6	1.1	0.6	0.58	0.6	0.6
Active material, at. %	S-10As	S-10As	S-10As	S-10As	S-10As	c	S-40As	S-40As	S-40As	S-40As
Wt. of active material, g	19.9	20.2	28.8	19.9	17.5	37.7	16.9	15.9	22.2	9.6
Electrode composition, wt %										
Active material	85.0	85.0	89.5	85	85	d	81.7	81.7	59.4	81.2
Carbon black	15.0	15.0	10.5	15	15		9.9	9.9		9.8
Porous graphite									21.8	
Molybdenum foam									12.7	
Electrolyte										
Thallium							8.4	8.4	6.1	9.0
Sheath	Graphite	Graphite	Graphite	W mesh	ZrO_2 cloth	Graphite	Graphite	Graphite	Graphite	Graphite
Thickness, cm	0.3	0.3	0.3	—	—	0.3	0.6	0.6	0.3	0.3
Temperature, °C	395	400	400	410	380	400	390	390	390	390-430
Theor. Cap. Density, A/cm^2	1.2	1.08	1.01	0.55	0.55	e	0.44	0.31	0.43	0.28
Maximum Performance										
Cap. density, $A\text{-}hr/cm^2$	0.23	0.13	0.13	0.08	0.172	0.03	0.15	0.11	0.11	0.17
% of theor. capacity	19.8	11.8	13.0	14.5	31.2	28.6	34.1	35.5	25.6	60.2
Current density, A/cm^2	0.1	0.1	0.1	0.005	0.005	0.035	0.1	0.04	0.1	0.05
Discharge cutoff voltage	1.0	1.0	1.0	1.0	1.0	1.0	1.0	1.0	1.0	1.0
Cell Life										
Hours	75	250	300	16	35	168	534	307	50	160
Cycles	46	8	17	1	1	32	105	58	22	24

TABLE II. (cont'd)

Cell No.	S-39	WS-7	WS-8	WS-9	WS-10	WS-11	WS-12	WS-13	S-40
Lithium Electrode									
Area, cm^2	113.1	100.0	154.0	100.0	100.0	100.0	100.0	45.7	100.1
Wt. of Li, g	5.6	5.6	9.7	6.1	8.2	8.6	9.0	10.3	7.5
Current collector	Ni	Ni	Ni	Ni	Ni	Ni	Ni	steel wool	SS
Thickness, cm	0.2	0.2	0.2	0.2	0.6	0.6	0.6	0.6	0.2
Sulfur Electrode									
Area, cm^2	24.7(II)	20.3(I)	46.0(IV)	20.3(IV,V)	20.0(IV)	20.0(III)	19.6(III,V)	19.6(III,IV)	20.3(I)
Thickness, cm	0.6	0.6	0.6	0.6	0.6	0.6[f]	0.6[f]	0.6[f]	0.6
Active material, at. %	S-40As	S-40As	S-40As	S-40As	S-40As	S-40As	S-40As	S-40As	S-23.7As
Wt. of active material, g	21.1	12.1	11.8	8.4	16.5	9.9	14.5	17.0	8.8
Electrode Composition, wt %									
Active material	90	71.3	46.3	68.5	36.4	90	90	90	90
Carbon black	10					10	10	10	10
Porous graphite		13.0	51.2	31.5					
Molybdenum foam					63.6				
Electrolyte		12.0							
Thallium		3.7	2.5						
Sheath	Graphite	Graphite	Graphite	ZrO_2 cloth	ZrO_2 cloth	Mo foam	Mo foam	Mo foam	Graphite
Thickness, cm	0.3	0.3	0.3	---	---	0.3	0.3	0.3	0.3
Temperature, °C	380	390	410	400	400	400	405	400	380
Theor. Cap. Density, A-hr/cm^2	0.50	0.37	0.16	0.26	0.51	0.31	0.45	0.54	0.42
Maximum Performance									
Cap. density, A-hr/cm^2	0.15	0.17	0.094	0.116	---	0.31	0.297	0.390	0.17
% of theor. capacity	30.7	43.7	58	44.8	---	100.0	65.6	72.0	47.7
Current density, A/cm^2	0.1	0.05	0.025	0.05	---	0.05	0.10	0.10	0.1
Discharge cutoff voltage	1.0	1.0	0.98	1.0	---	1.0	0.95	0.95	1.0
Cell Life									
Hours	30[g]	310	140	68	1.0	275	317	15	170
Cycles	5	45	23	8	0	82	109	2	28

[a] A description of current-collector and sheath materials is given in Table III.

[b] Indicates type of electrode design. Areas given are projected areas on lithium electrode (not contact area between sulfur, electrolyte, and (current collector).

[c] Active material for Cell WS-6 was discharged product from Cell WS-5.

[d] Based on initial composition of Cell WS-5, S concentration would be 68 wt %, but chemical analysis showed 3.6 wt % S.

[e] 0.1 A-hr/cm^2, based on sulfur analysis.

[f] Total thickness; electrode material was convoluted, as in Fig. 2.

[g] After termination of operation of Cell S-39, the sulfur electrode was removed and tested in a cell sealed with gaskets for 120 hr and 16 cycles.

either charge or discharge. Usually, discharge data were taken from the fully charged condition (open-circuit voltage of 2.3 V), and charge data were taken from the partially discharged condition. The cell voltage was measured as a function of time during charge and discharge. These data were used to calculate voltage-*vs.*-capacity density curves. The total capacity (A-hr) for the charge and discharge half-cycles were determined electronically using a Lectrocount Integrator.* Over the operating life of the cells, which for many cells was hundreds of cycles and hundreds of hours, variables such as cell voltage, current, charge and discharge time, and temperature were monitored by an automatic data-acquisition system with punched-tape output. The tapes were fed to a computer to perform the calculations and to produce the voltage-*vs.*-capacity density curves mentioned above.

TABLE III. Current-Collector and Sheath Materials Used in Lithium/Sulfur Cells

Material	Designation	Porosity, %	Pore Size, μm	Particle Size, μm	Surface Area, m^2/g
		Sulfur-Electrode Current Collector			
Carbon black	Vulcan XC-72R[a]			0.015	230
Carbon black	Gould[b]				970
Graphite	PG-25[c]	48	120		
Graphite	PG-60[c]	48	33		
Graphite	FPA-20[c]	91	26-80		
Mo foam		78	25		
		Lithium-Electrode Current Collector			
Nickel	Feltmetal[d]	80	60		
Stainless steel	Feltmetal[d]	90			
Steel wool		97.5			
		Sheath			
Graphite	PG-60[c]	48	33		
Mo foam		75	25		
ZrO_2 cloth	ZYW-30[c]				
W mesh					

[a] A product of Cabot Corporation.

[b] Sample received from Gould Laboratories.

[c] A product of Union Carbide Corporation.

[d] A product of Brunswick Corporation.

* A product of Royson Engineering Co.

A discussion of the cell experiments is given below.

1. Sulfur-10 at. % Arsenic Sulfur-Electrode Mixtures

Cells S-31 to S-34 and WS-4 to WS-6 were operated with S-10 at. % As mixtures in the positive electrode. These mixtures were prepared either by adding the arsenic gradually to the sulfur while stirring the material at 300°C or by sealing the sulfur and arsenic in an evacuated quartz capsule and heating to 500°C for 100 hr with frequent agitation. All of the cells operated with these sulfur-arsenic mixtures experienced high losses of sulfur (90% or greater) from the positive electrode, and the next series of cells was operated with substantially higher arsenic concentration in the sulfur electrode. Recent information has indicated, however, that the arsenic used in the preparation of the S-10 at. % As mixtures may have been coated with an oxide film that largely prevented alloy formation; thus, the arsenic would not have been effective in lowering the sulfur vapor pressure. (This problem is discussed further in Sections II.C.2 and 3, below.)

The performance characteristics of Cells S-31 and WS-4 to WS-6 are discussed below; these results are typical of the other cells that contained the S-10 at. % As mixture.

Cell S-31. Cell S-31 was operated for 75 hr and 46 cycles. The short-time peak power density was 1.1 S/cm^2. A capacity density of 0.23 A-hr/cm^2 (19.8% of theoretical) was measured for Discharge 1 at 0.1 A/cm^2 to a 1.0-V cutoff.* The resistance overvoltage at the beginning of this discharge was was 0.075 V, but increased to 0.3 V near the end of the discharge. A similar increase in the resistance overvoltage was observed during discharge. The cause of this behavior was not determined. Some difficulty was experienced in charging the cell during Cycle 1. The 2.85-V charge cutoff voltage (2.6 V, IR-free) was eventually reached, but the ampere-hour efficiency for the next discharge was 19.6%. This behavior may have been caused by lithium shorting, but the cause could not be confirmed by examination of the cell.

The capacity density of Cell S-31 decreased with cycling; after 5 cycles, a decrease to 0.06 A-hr/cm^2 (5.4% of theoretical) at 0.1 A/cm^2 to a 1.0-V cutoff had occurred. This value, which was 25% of that measured for Cycle 1, remained constant for 46 cycles, at which time, operation of the cell was terminated. The sulfur concentration in the positive electrode had decreased from 68 to 2.2 wt % during cycling of the cell. This high sulfur loss is consistent with the low capacity density measured just prior to terminating the cell test. Examination of the cell also showed some voids in the sulfur electrode; apparently, some gas had been trapped within the electrode. The possible effect of this trapped gas on sulfur containment has not been determined.

Cells WS-4 to WS-6. These cells were operated in a series of experiments designed to test the concept of electrochemically discharging sulfur electrode materials to allow vacuum-degassing of the cell assembly before sealing, by utilizing the low vapor pressure of sulfur in the discharged state.

---

*All discharge cutoff voltages are IR-included.

Cells WS-4 and WS-5 used Type VI sulfur electrodes and the cell configuration shown in Fig. 6. The current collector material in the sulfur electrodes of both cells was Vulcan carbon black (15 wt %) in a mixture with the S-10 at. % As material. The S-As-C mixture was pressed into a tungsten screen basket for Cell WS-4 and discharged at 0.005 A/cm^2 to obtain a deep discharge (greater than 50% of the theoretical capacity density). The discharged sulfur electrode products were not contained in the mesh basket and formed a deposit between the sulfur electrode and lithium electrode, as shown in Fig.7. Chemical analysis of the deposit showed that it contained a large percentage of Li_2S.

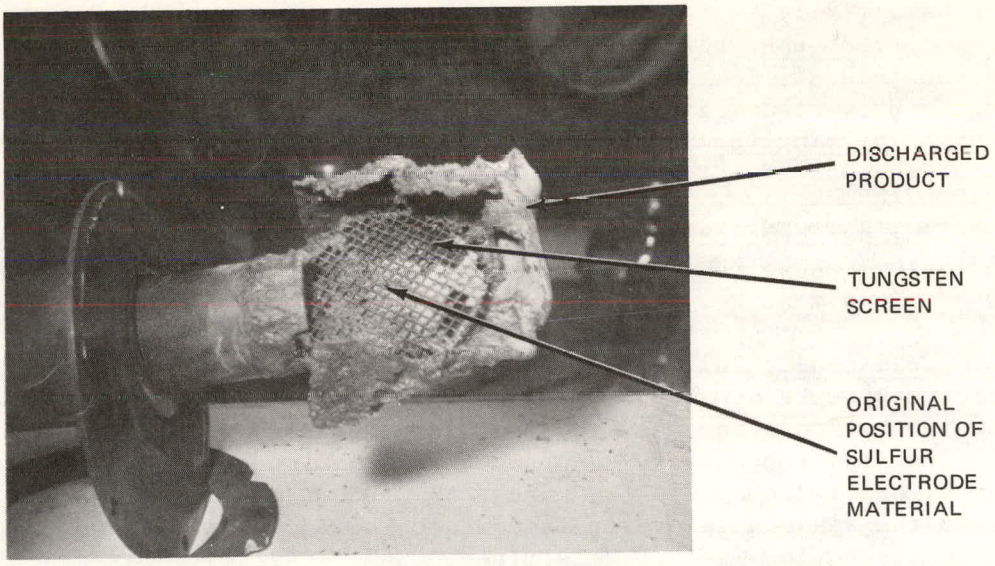

Fig. 7. Discharged Products for Cell WS-4

Cell WS-5 used a sulfur electrode similar to that of Cell WS-4 except that a layer of zirconia cloth* was used between the sulfur-containing material and the tungsten screen basket in an attempt to confine the discharged sulfur electrode products. The cell was discharged at 0.005 A/cm^2 to a cell voltage of 1.0 V, and the sulfur electrode was removed from the cell. Visual examination indicated that the sulfur-electrode material had been contained within the electrode structure. This material was ground to a fine powder and incorporated into a Type II sulfur electrode. The Type II electrode was operated in Cell WS-6 in the configuration shown in Fig. 4, but without the upper lithium electrode. Cell WS-6 was vacuum-degassed while submerged under molten electrolyte at 450°C with no sign of sulfur fumes, thus indicating that free sulfur was not present. The electrical performance of this cell was poor (only 3.5% of the sulfur theoretically available from the starting material for Cell WS-5 was utilized); subsequently, a chemical analysis of a sample of the sulfur electrode material of Cell WS-6, taken prior to the electrical performance tests, showed that greater than 91% of the sulfur originally contained in the Type VI sulfur electrode of Cell WS-5 had been lost from the electrode structure during the slow discharge. Because of the high loss of sulfur-containing materials during discharge, efforts to prepare discharged sulfur electrode

*A product of Union Carbide Corp., Type ZYW-30.

materials using Type VI sulfur electrodes and S-10 at. % As the starting material were discontinued.

2. Sulfur-40 at. % Arsenic Sulfur-Electrode Mixtures

Cells S-35 to S-39 and WS-7 to WS-13 were operated using S-40 at. % As (plus carbon) electrode mixtures. The purpose of these experiments was to determine the effect of a large increase in the arsenic content on the performance, lifetime, and cycle life of lithium/sulfur cells. The arsenic content in these cells was four times that used in earlier tests. Increasing the arsenic content to the highest feasible arsenic content, considering specific energy, appeared to be the fastest means of evaluating the effectiveness of arsenic in lowering the sulfur activity and preventing sulfur escape from the sulfur electrode. Results from these cells indicated that the S-40 at. % As composition was effective in reducing sulfur losses from the sulfur electrode to the extent that sulfur utilizations greater than 30% were sustained for hundreds of hours and hundreds of cycles, and sulfur utilizations greater than 70% were measured for a few cycles. The performance limitations of these cells are now believed to be associated with problems in the sulfur-electrode design, *e.g.*, the need to optimize the contact area of the sulfur, electrolyte and current collector, rather than sulfur escape from the sulfur electrode.

Two methods were used to prepare the mixtures of carbon black and S-40 at. % As. In the first technique, sulfur and arsenic in the proper proportions were sealed in an evacuated quartz capsule, along with ∿2.5 at. % Tl, to lower the viscosity of the melt,[4] and the mixture was heated at 400°C for about 100 hr with frequent mixing. This mixture was then removed from the quartz capsule, heated to about 350°C, and mixed with the carbon at that temperature. In the second method, commercially available As_2S_3* and carbon were mixed with a mortar and pestle at room temperature. No significant difference was found in the performance of cells using these two mixtures. Therefore, the use of As_2S_3 is preferred because it does not require the use of another additive such as thallium.

The performance of Cells S-35, S-38, S-39, and WS-11 to WS-13 is discussed below. These results are typical of the other cells which contained the S-40 at. % As mixture.

Cell S-35. Cell S-35 was operated for 534 hr and 105 cycles. The cell was cycled continuously with constant-current discharging and either constant-current or constant-voltage charging. This cell demonstrated less decrease in capacity density with cycling than did previous cells. The capacity density as a function of cycle number is shown in Fig. 8. The cause of the gradual decline in capacity density with cycling after hundreds of hours of operation was not determined, but is believed to be the result of corrosion of the electrical insulators and subsequent lithium shorting. This hypothesis is consistent with the observation that the ampere-hour efficiency of the cell decreased over the long operating period. The cell was operated at discharge current densities of 0.04, 0.1, and 0.2 A/cm^2. The capacity densities measured at these current densities to a 1.0-V cutoff were 0.21, 0.15, and 0.08 A-hr/cm^2, respectively. These capacity densities correspond to 47, 34.1, and 21.1% of

*A product of Alpha Products of Ventron Corp.

the theoretical capacity density, respectively, based on Li_2S as the discharge product.

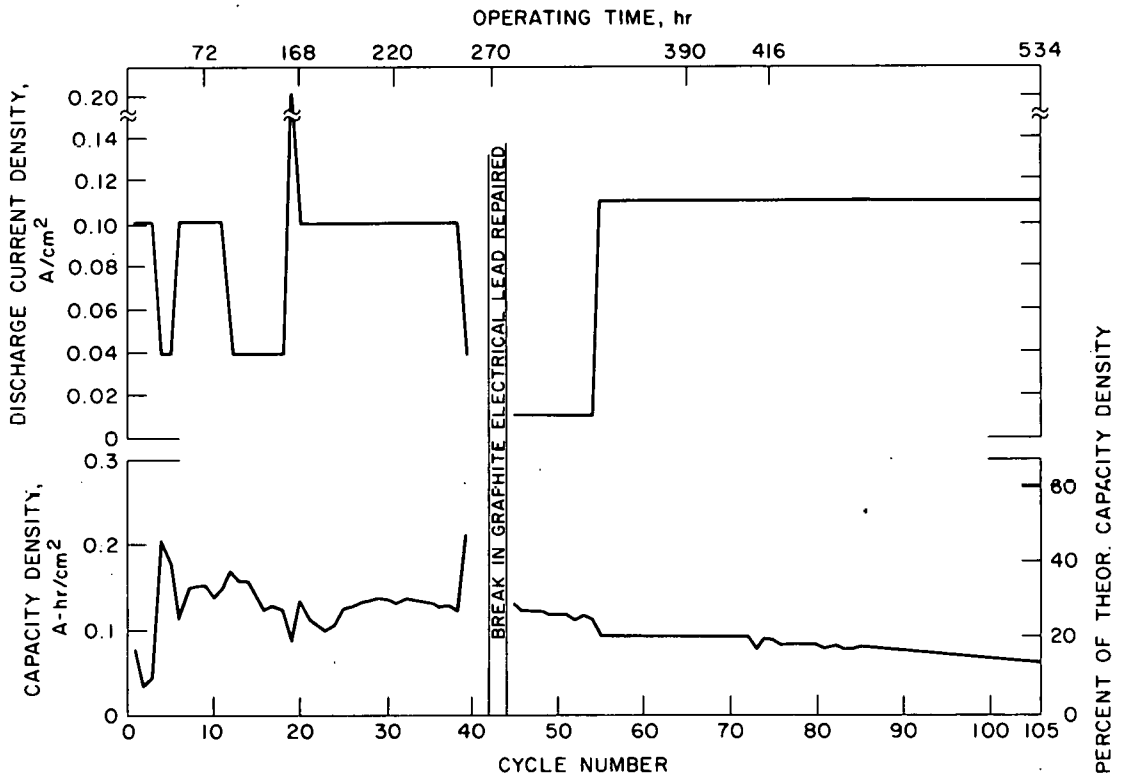

Fig. 8. Capacity Density as a Function of Cycle Number for Cell S-35 (temperature, 390°C)

The short-time peak power density for Cell S-35 was about 2.5 W/cm^2, a value that exceeds the goal of 1 to 2 W/cm^2 for this program. The resistance overvoltage at a 4-A discharge current was about 0.1 V. The initial current density through the cell during constant-voltage charging was nearly 1 A/cm^2. Examination of the cell after 270 hr indicated that a small fraction of the lithium originally loaded in the cell was not contained in the nickel Feltmetal. Also, examination of the sulfur electrode indicated that the graphite lead used to conduct current from the cell was broken. After the current lead was replaced, operation of the cell was continued. The high current density during constant-voltage charging appeared to be detrimental to the lithium retention in the Feltmetal and to the structural stability of the graphite current lead. In future experiments using constant-voltage charging, the current density will be limited at the start of the charge.

Constant-voltage charging was used for Cell S-35 during Cycles 24 to 72. Further data are needed to conclude whether constant-voltage or constant-current charging is the more effective charge mode.

After 534 hr of operation, the sulfur electrode of Cell S-35 contacted the lithium electrode owing to the failure of the graphite supporting rod. As a

result, the sulfur electrode was destroyed and the sulfur-electrode material was not available for chemical analysis.

Cell S-38 and WS-11 to WS-13. The purpose of operating these cells was to determine the effect on cell performance of increasing the contact area between the sulfur, electrolyte, and graphite current collector in the sulfur electrode. Operation of Cells WS-11 to WS-13 had the additional objective of evaluating the effectiveness of electrolyte-wetted molybdenum foam as a barrier to physical losses of active material from the sulfur electrode.

The PG-60 porous graphite (infiltrated with electrolyte) used in Cell S-38 (Type I electrode) had thirty-one 1/4-in.-dia holes to contain the sulfur-electrode mixture. The ratio of the contact area to the sulfur-electrode volume was 20 cm^{-1} compared with a value of 12 cm^{-1} for Cell S-35, which had seven 1/2-in.-dia holes to contain the sulfur-electrode mixture. Cells WS-12 and WS-13 had Type III sulfur electrodes in which radial grooves were machined into the molybdenum foam current collector. This method of construction gave a ratio of surface area of contact to volume of active material of 40 cm^{-1}. These cells also contained a reference electrode (Type V) to determine the cause of performance losses by monitoring the lithium electrode independently.

Cell S-38 was operated for 160 hr and 24 cycles. A plot of capacity density *vs.* cycle number is shown in Fig. 9, and representative charge-discharge curves are shown in Fig. 10. Cell S-38 was cycled at a relatively constant capacity density of about 0.14 A-hr/cm^2 (50% of the theoretical capacity density) at a discharge current density of 0.05 A/cm^2 to a 1.0-V cutoff (the highest capacity density was 0.16 A-hr/cm^2 in Cycle 8). This low discharge current density was used to obtain cell performance characteristics with depp discharge.

The temperature of Cell S-38 was increased from 390 to 430°C at Cycle 11 to determine the effect of temperature on cell performance. At this point, the ampere-hour efficiency increased from about 50 to 80%, the capacity density increased from about 0.12 to 0.14 A-hr/cm^2, and the average discharge voltage increased by about 0.2 V. (Before the temperature increase, the capacity density had decreased from 0.16 to 0.12 A-hr/cm^2 with cycling.) The cause of this cell behavior was not determined. The effect of temperature on performance will be investigated further in future cells.

Approximately 100% of the theoretical capacity was measured for Cell WS-11 during Discharge 1 at a current density of 0.05 A/cm^2 to a cutoff voltage of 1.08 V. The discharge current density was then increased to 0.10 A/cm^2. Cell performance with time is shown in Fig. 11. The percent of theoretical capacity reached a steady value of 37.5% and did not drop further until electrical short-circuiting, as evidenced by a further decline in ampere-hour efficiency were caused by intermittent electrical short circuits.) A discharge at 0.05 A/cm^2 during the lifetime test (Cycle 37) did not result in an increase in capacity. This may indicate that substantially all of the remaining cell capacity was being utilized at 0.1 A/cm^2, or that some change had occurred in the electrode that limited deeper penetration and, consequently, lowered the sulfur utilization. The feedthrough insulator failed after 46 cycles and 200 hr, probably as a result of corrosion by the lithium; however, testing of the sulfur electrode was continued with a new lithium electrode. Cell performance with the second lithium electrode decreased with time, and the cell failed

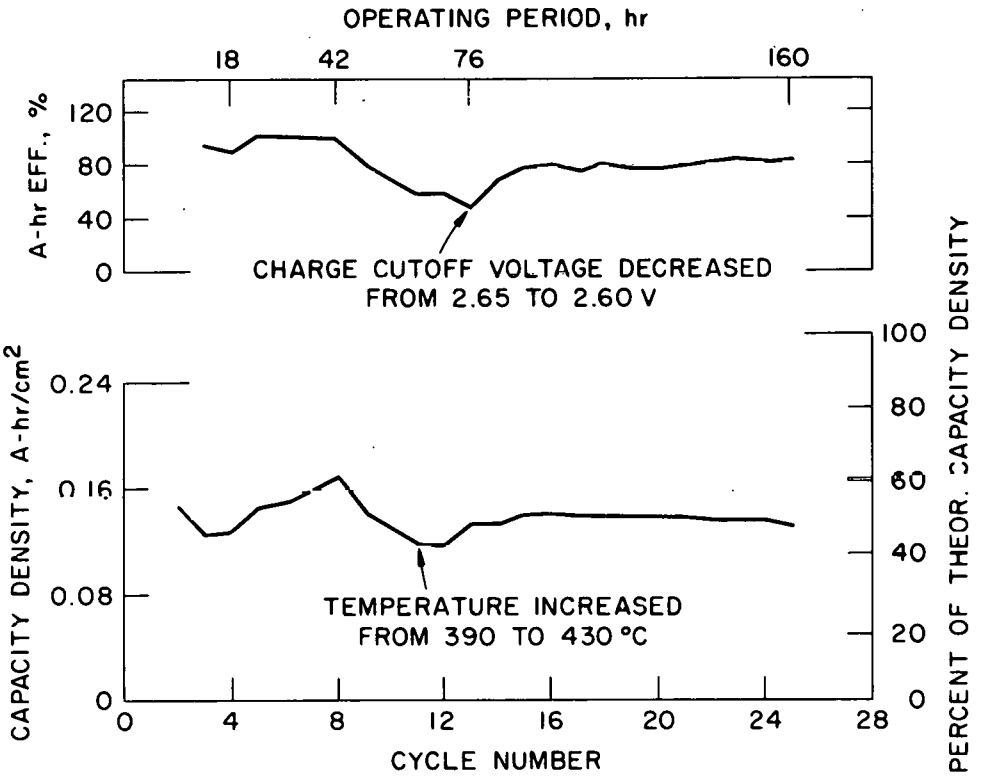

Fig. 9. Capacity Density as a Function of Cycle Number for Cell S-38 (temperature, 390-430°C; current density, 0.05 A/cm^2)

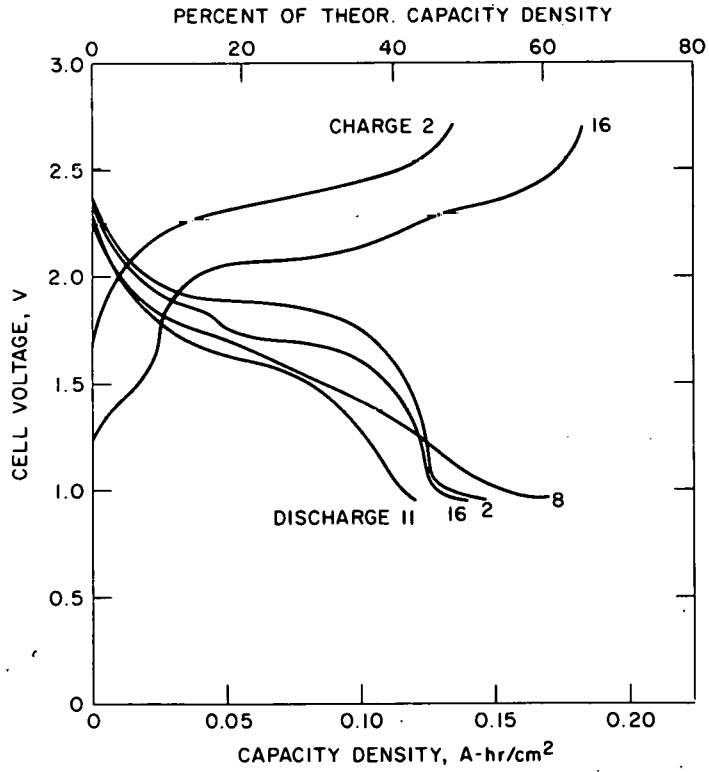

Fig. 10.

Voltage-Capacity Density Curves for Cell S-38 (temperature 390-430°C; theoretical capacity density, 0.28 A-hr/cm^2; current density, 0.05 A/cm^2)

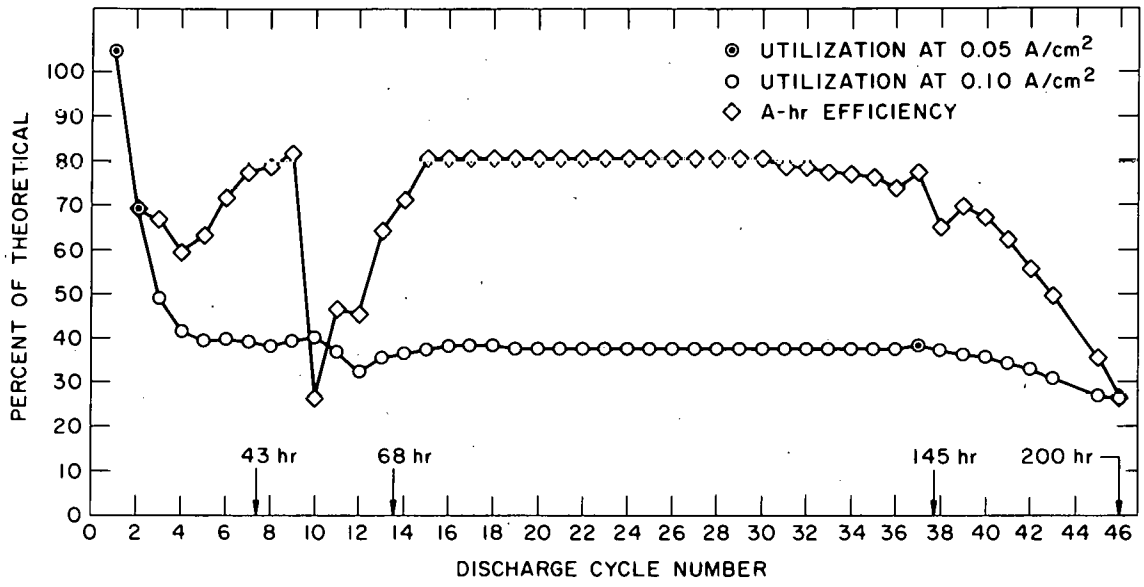

Fig. 11. Sulfur Utilization and Ampere-Hour Efficiency *vs.* Discharge Cycle Number for Cell WS-11 (temperature, 400°C; theoretical capacity density, 0.31 A-hr/cm^2)

because of an electrical short circuit.

Cell WS-12 was identical to Cell WS-11 except that a reference electrode containing its own supply of sulfur was used to distinguish between sulfur-electrode and lithium-electrode degradation. The initial discharge at 0.1 A/cm^2 current density, utilized 65.6% of the sulfur present. The utilization dropped with time and stabilized at 20% for 80 cycles and 250 hr, while the ampere-hour efficiency stabilized at 75-80%, as shown in Fig. 12.

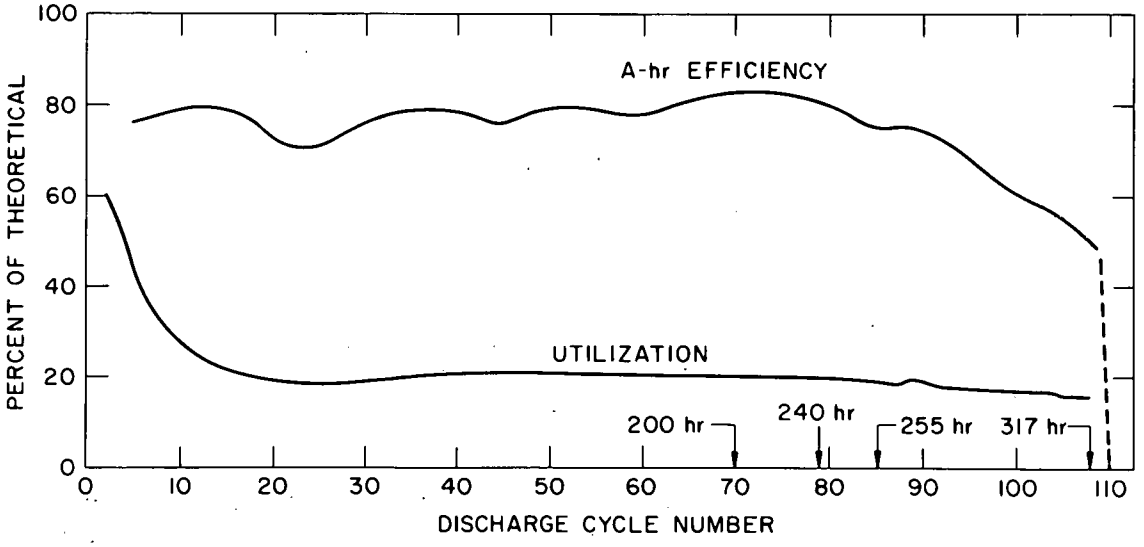

Fig. 12. Sulfur Utilization and Ampere-Hour Efficiency *vs.* Discharge Cycle Number for Cell WS-12 (temperature, 405°C; theoretical capacity density, 0.45 A-hr/cm^2)

The cell appeared to develop an electrical short circuit when a power failure resulted in the freezing of the electrolyte and destruction of the sulfur electrode. During operation, the reference electrode appeared to be stable and indicated that the loss in cell performance resulted, at least partially, from poor lithium-electrode performance; contamination of the lithium electrode with sulfur reactants is a possible cause of the poor performance. This behavior is illustrated in Fig. 13, in which the cell voltage and reference voltage are compared during Discharges 1, 3, 9, and 17. During the first discharge, the reference electrode maintained a stable open-circuit voltage until the very end of discharge when the reference voltage dropped sharply and continued to fall while the cell was on open circuit. This decrease may have resulted from a release of reactants from the sulfur electrode, which in turn, caused a reduction of the lithium-electrode activity and a lowering of the reference voltage. In Discharge 3, an earlier break occurred in the reference voltage, and by Discharge 9, the reference voltage began to decrease simultaneously with the onset of discharge. A further observation is that the mean reference voltage gradually decreased with time. This gradual decrease may be ascribed to either of the following causes: (1) a slow discharge of the reference electrode due to the very small current drawn by the recorder or (2) a polarization of the lithium electrode due to poisoning of the lithium electrode surface opposite the reference electrode. (The reference electrode faces the centermost portion of the lithium electrode.)

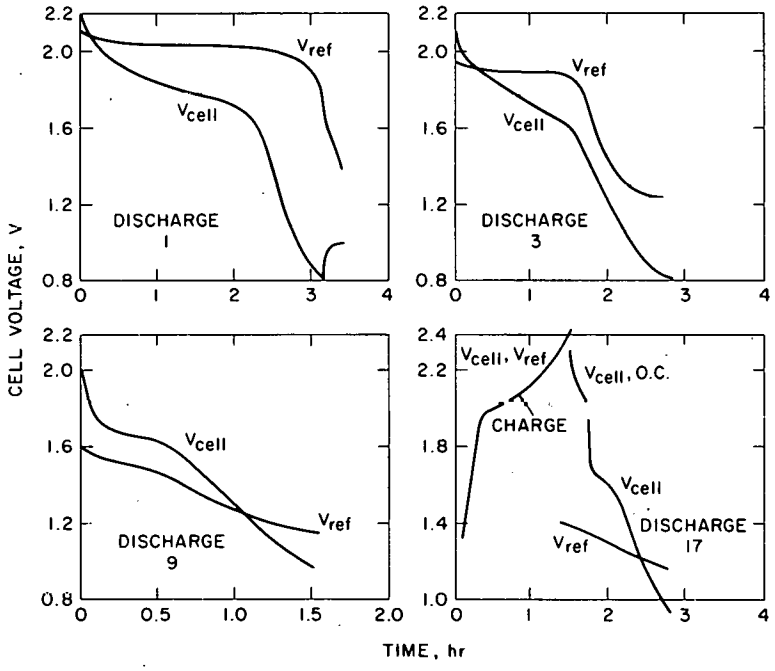

Fig. 13. Cell and Reference Voltages During Discharge as Functions of Cell Life for Cell WS-12 (temperature, 405°C)

A test was performed during Cycle 17 to determine whether one of the above explanations was probable. After discharge, the reference electrode was connected in parallel to the working sulfur electrode during the charge cycle.

This procedure should have charged the reference electrode and resulted in a higher open-circuit voltage if the decrease in the reference voltage had been caused by discharging of the reference electrode by the current drain from the recorder. A decrease in the reference cell voltage caused by a poisoning of the lithium electrode should not have been affected by the charging procedure. As shown in the cell performance curves of Fig. 13, the reference cell voltage did not increase after the charge, thus indicating that the lithium electrode might have been partially poisoned. This would suggest that a portion of the cell-performance decline was due to the deterioration of performance of the lithium electrode. Examination of the lithium electrode after disassembly of the cell revealed a uniform red coating over the surface of the electrode. It is believed that this material contained a large quantity of lithium sulfide. A large amount of lithium still remained in the Feltmetal.

Cell WS-13 was constructed with a sulfur electrode identical to that of Cell WS-12, but the lithium was impregnated in a structure of steel wool enclosed in stainless steel screen, rather than in nickel Feltmetal, to determine whether a structure with larger pores would provide improved lithium retention. The cell voltage *vs.* cell capacity during discharge is shown in Fig. 14.

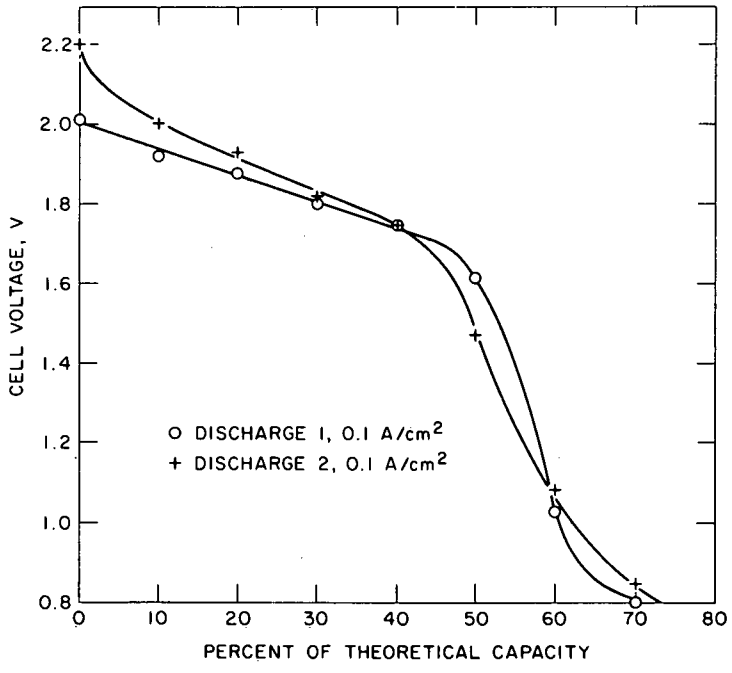

Fig. 14. Cell Voltage *vs.* Percent of Theoretical Capacity During Discharge of Cell WS-13 (temperature, 400°C; theoretical capacity density, 0.55 A/cm^2)

The first discharge at 0.1 A/cm^2, utilized 70.8% of the theoretical capacity density and yielded a capacity density of 0.37 A-hr/cm^2. The performance improved slightly on the second discharge (72.0% of the theoretical capacity density, 0.39 A-hr/cm^2), but shorting occurred during the subsequent charge and the cell test was terminated. Examination of the components revealed that the molybdenum-foam housing of the sulfur electrode had broken from the

supporting current-collector lead, and several large drops of lithium had escaped from the steel wool and were present in the electrolyte. The performance of this cell was very close to the cell performance goals (0.4 A-hr/cm^2, 70% utilization, 0.1 A/cm^2) for automotive applications. These performance figures will be used in design calculations to determine the specific energy (W-hr/kg) that could be obtained with cells having a Type III sulfur-electrode configuration.

The performance data of these cells indicate that the increase in contact area of the sulfur, electrolyte, and current collector in Cells S-38 and WS-11 to WS-13 improved the sulfur utilization compared with that of Cell S-35.

Cell S-39. This cell, which had a theoretical capacity of 12.5 A-hr, was the first welded cell tested in the NSF program. The cell components and their weights are given in Table IV. The cell-assembly operation was conducted satisfactorily, but a number of problems were encountered in welding the cell.

TABLE IV. Weights of Components of Welded Cell S-39

Cell Components	Weight,[a] g
E-Brite stainless steel cover	35.1
E-Brite cup	74.2
Graphite housing	47.3
Zirconia fabric	3.6
Molybdenum adapter	0.9
Alumina insulator	4.0
Nickel Feltmetal	36.4
Molybdenum-mesh current collector	6.5
Lithium	5.6
Sulfur electrode mixture	21.1
LiF-LiCl-KCl electrolyte	151.4

[a]The total cell weight was about 0.39 kg.

A copper chill block that was used to remove heat from the welded area provided insufficient heat conduction, and the welded area overheated. The helium atmosphere in the glovebox also contributed to the cell overheating. The copper chill block could not be removed from the cell after welding. Because the heat produced during the welding operation apparently caused no damage to the cell and because the copper chill block was ineffective, a copper block will not be used during the welding operation for the next welded cell.

A capacity density of 0.22 A-hr/cm^2 (43.2% of the theoretical capacity density) was measured at a discharge current density of 0.05 A/cm^2 to a 1.0-V cutoff during Discharge 1. The discharge current density was increased to 0.10 A/cm^2 for Discharge 2 and a capacity density of 0.15 A-hr/cm^2 (30.7% of the theoretical capacity density) was measured to a 1.0-V cutoff. An electrical short circuit developed in the cell during Charge 2.

The cause of the electrical short circuit has not been determined; how-

ever, further examination of the cell components is planned to determine whether the shorting may have resulted from free lithium or possibly from a conductive film formed on the electrical feedthrough.

The next welded cell will be operated when ceramic separators and feedthroughs that are stable in the cell environment are available. These cell components are presently being tested in gasketed, sealed lithium/sulfur cells.

3. Sulfur-23.7 at. % Arsenic Sulfur-Electrode Mixtures

Cell S-40. This cell was operated with a positive-electrode mixture of S-23.7 at. % As and carbon black. Since one goal of these investigations is to develop cells with the highest specific energy (W-hr/kg) possible, it is desirable to minimize the weight of arsenic in the cells. The principal objective of this cell test was to determine whether an arsenic concentration lower than 40 at. % (the concentration used in the preceding tests) would provide effective sulfur containment and, thus, sustained capacity density with cycling.

A second objective of this cell test was to investigate the use of stainless steel Feltmetal as a current collector in the lithium electrode. In earlier cells, nickel Feltmetal was used as the lithium-electrode current collector; however, this material is costly, and has not demonstrated adequate lithium containment upon prolonged cycling. Recent laboratory investigations (see Section III) have indicated that lithium electrodes with steel wool current collectors perform well when cycled against a lithium-aluminum electrode for a large number of cycles. Accordingly, various types of steel current collectors will be tested in cell environments.

A third objective of this experiment was to test a different technique for preparing sulfur-arsenic mixtures than was used in earlier cells. The preparation procedure consisted of heating As_2S_3-sulfur mixtures at 400°C in an evacuated quartz capsule for several hours with frequent mixing.

Cell S-40 was operated for 28 cycles and 100 hr. A capacity density of 0.17 A-hr/cm^2 (47.7% of the theoretical capacity density) was measured at 0.1 A/cm^2 discharge current density to a 1.0-V cutoff. For the remaining cycles, a one-hour rate of about 0.1 A/cm^2 was demonstrated. Although this capacity density does not meet the goals of the program, the nearly constant capacity density demonstrated during the operating period of 100 hr suggests that an arsenic concentration lower than 40 at. % may provide effective sulfur containment. Operation of Cell S-40 was terminated after a power failure and subsequent freezing of the electrolyte. Sulfur analyses for this cell were not available at the writing of this report.

D. Summary and Conclusions

Short-time peak power densities greater than the goal of 1 to 2 W/cm^2 have been achieved with positive electrodes consisting of sulfur-arsenic-carbon mixtures in graphite housings. Moreover, the sulfur utilization goal (70% of the theoretical capacity density at 0.1 A/cm^2 to a 1.0-V cutoff) has been exceeded for a few cycles. A capacity density of 0.1 A-hr/cm^2 (about 30% of the theoretical capacity density) has been sustained at a discharge current density of 0.1 A/cm^2 to a 1.0-V cutoff for an operating period of over 500 hr

and 100 cycles. This performance represents significant progress over the performance of earlier cells operated in this program.

The major areas of investigation which appear to require further effort in order to develop longer-lived cells with the performance required for vehicle propulsion are lithium containment in the current collector and higher sulfur utilization (70% of theoretical capacity) for hundreds of hours and hundreds of cycles. In the latter area, cells having positive electrodes of iron sulfide (FeS_2 or FeS) will be investigated. Such cells have shown good electrical performance in recent laboratory studies in the AEC program.[5] Effort will also be directed toward demonstrating the corrosion resistance of feedthroughs and separators in the cell environment.

Conclusions drawn from experiments conducted during this reporting period are as follows:

1. A significant improvement in sulfur containmement has been demonstrated in cells having a S-40 at. % As mixture in the positive electrode, compared with cells having a S-10 at. % As mixture. One cell (S-40) with S-23.7 at. % As also showed improved sulfur retention, but the minimum arsenic concentration required for adequate sulfur retention over long periods of time has not been established.

2. Nickel Feltmetal current collectors appear to be inadequate for completely containing the lithium in the negative electrode for many hundreds of cycles under the present operating conditions.

3. Electrolyte was displaced by sulfur mixtures in the porous graphite sheath that is part of the housing of the sulfur electrode. A material that is preferentially wet by electrolyte is needed to contain particulates, such as the carbon current collector, in the sulfur electrode.

4. Electrical feedthroughs using calcium zirconate insulators are suspected to have inadequate corrosion resistance in the cell environment.

5. Sulfur electrodes (Types I and III) with increased areas of contact between the sulfur, electrolyte, and current collector have provided increased sulfur utilization in test cells.

6. Results from cells having reference sulfur electrodes appear to indicate that the decline in performance of some cells can be attributed, not only to problems with the sulfur electrode, but to problems with the lithium electrode as well.

III. SUPPORTING LABORATORY STUDIES
(R. K. Steunenberg)

A. Lithium-Electrode Development Studies
(D. R. Vissers)

Investigations are being conducted on the lithium-retention characteristics of porous support materials for use in the negative electrodes of lithium/sulfur cells. To prevent short-circuiting of the cell by the liquid lithium, it is essential that the lithium be absorbed readily by the electrode support material when the cell is recharged. New porous support materials are being sought, and the factors that influence their retention of lithium are being studied.

1. Lithium-Electrode Support Materials

The lithium electrodes in the cells of practical high-specific-energy batteries will probably be about 0.5 cm thick. Nickel and stainless-steel Feltmetals, the support materials that have been used most frequently for lithium electrodes in the experimental cells, may be too costly for use in practical batteries; moreover, recent cell tests (see Section II.C) have suggested that the retention of lithium by these Feltmetals may be inadequate in long-term use. Accordingly, an investigation is being performed to identify and evaluate alternative support materials for the liquid lithium. Several potential support materials are listed in Table V. The void volumes of these materials are similar (∿90%); however, steel wool and expanded metal (stainless and mild steels) have the lowest cost. Consequently, the lithium-retention characteristics of steel wool and expanded metal are being investigated first.

TABLE V. Potential Support Materials for Lithium Electrodes

Material	Form	Source	Void Volume, %	Cost per Sq. Meter,[a] $
Nickel	Feltmetal	Brunswick Corp., Milford, Conn.	∿90	300
Stainless steel	Demister	Otto York Co., New York, N.Y.	∿85[b]	100
Stainless steel	Expanded metal	Die Mesh Corp., Pelham, N.Y.	∿90[b]	100
Mild steel	Expanded metal	Die Mesh Corp., Pelham, N.Y.	∿90[b]	100
Nickel or iron	Foam metal	Hogen Industries, Willoughby, Ohio	∿90	250
Steel	Wool	James H. Rhodes, Chicago, Ill.	∿90[b]	<10

[a] Costs are for materials 0.5 cm thick in lots of ∿50 kg. Costs would probably be markedly reduced for the large quantities that would be required for battery production.

[b] As compressed to a suitable density for use in a lithium electrode.

Stainless steel expanded metal and two types of steel wool (Type "0" and Type "2") were used to fabricate electrode structures approximately 0.5 cm thick and about 2.5 cm in diameter. A 20-mesh mild steel screen was used on both sides of the electrode to contain and support the steel wool. The lithium-loading capacity of these structures was tested by immersing them in liquid lithium at 500°C until the support material was wet and apparently filled by the lithium. Essentially complete (>97%) filling of the void spaces in all the three materials was achieved.

2. Lithium-Retention Studies

The lithium-retention characteristics of a steel-wool lithium electrode were investigated at 400°C in an electrochemical cell in which lithium was cycled between the test electrode and a lithium-aluminum counterelectrode.[6] This Li/LiCl-KCl/Li(Al) cell was contained in a specially designed closed system (containing helium) that permitted control of the cell atmosphere and the addition of various materials to the system.

The support material for the test electrode was Type "0" steel wool that was contained in a 20-mesh mild steel screen to form a structure 2.54 cm in diameter and ∿0.5 cm thick. The steel wool, which had a void volume of 84.7%, was loaded with 0.811 g of lithium (equivalent to a capacity of 3.13 A-hr). The lithium-aluminum electrode was fabricated from continuous aluminum fiber* 0.10 mm in diameter formed into a disk 3.8 cm in diameter. Sandwiched within this disk was the spiral-shaped end section of a 3.2-mm-dia stainless steel electrode lead. The aluminum disk was located in a tantalum crucible where it was held in place by two 20-mesh stainless steel end pieces. The components of this electrode were held together by 0.2-mm-dia nickel-chromium wire. The lithium-aluminum alloy was formed in the electrode electrochemically during the first discharge of the lithium electrode. The electrolyte in this cell consisted of 111.3 g of LiCl-KCl eutectic (m p, 352°C). A schematic diagram of the completed cell is shown in Fig. 15.

The lithium initially present in the lithium electrode was partially cycled between the two electrodes seventeen times to evaluated the lithium-retention properties of the steel wool support material. About 67% of the total lithium present was cycled each time during the first twelve cycles, and about 25% each time during the last five cycles. The current density during the charge portion of a cycle (transfer of lithium to the lithium electrode) was varied from 50 to 400 mA/cm^2. During discharge, the current density was varied from 50 to 200 mA/cm^2. The cell voltage did not exceed +0.9 V during charging, nor drip below -0.33 V during discharging. The nominal resistance of the cell was 0.25 $\pm$ 0.01 ohm. During these initial cycling studies, the steel wool electrode performed very satisfactorily.

In the second portion of the study, the effect of moisture on the operating characteristics of the test electrode was investigated. After Discharge 17, 10 ppm of water by weight was added to the LiCl-KCl electrolyte by injecting a known quantity of helium saturated with water vapor into the evacuated cell system. After Discharge 18, 40 ppm of water vapor was added

* A product of the Brunswick Corp.

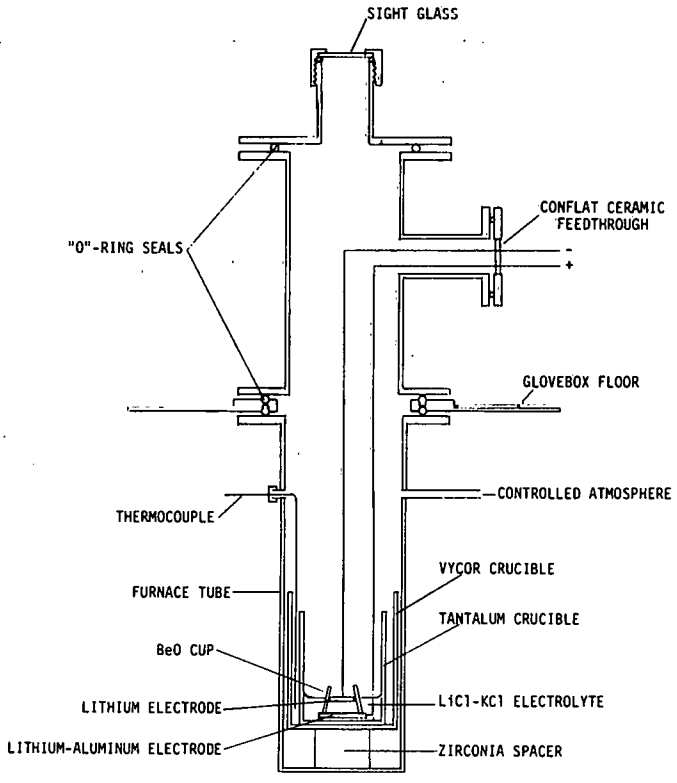

Fig. 15.

Cell for Lithium-Retention Studies

to the electrolyte, followed by two additions of 50 ppm each after Discharges 19 and 21. No deterioration in the cell performance, relative to the cell resistance or the charge-discharge capacity balance, was detected through Charge 23. About one third of the lithium was cycled during Cycles 17 through 20. The time interval between Discharges 18 and 23 was approximately seven days.

During Discharge 24, an attempt was made to carry out a 2 A-hr discharge (67% of the theoretical capacity); however, the discharge capacity of the cell, at this point, was found to be 1.89 A-hr.

After Charge 24 and Discharge 25, water vapor was again added to the cell, each addition corresponding to about 100 ppm in the electrolyte. At this point, the cell capacity began to decrease rapidly and continued to drop after each charge, thereby indicating that either lithium was being lost from the lithium electrode during charging or the lithium-aluminum electrode was being made inactive by reaction of the active aluminum surface with the added water. After Charge 29, the capacity of the cell had dropped to about 0.30 A-hr, or about 10% of the theoretical value. At this point, the test was terminated.

The distribution of lithium in the cell after it was disassembled is shown in Table VI. The lithium was determined by acid-base titration on the assumption that 1 meq of base, formed during aqueous hydrolysis, indicated the presence of 1 meq of lithium. The data in Table VI indicate that 0.506 g of lithium (corresponding to 1.96 A-hr) was present in the cell (anode, cathode, and electrolyte) at the completion of the above test. These results imply that 0.263 g (1.02 A-hr) of lithium had disappeared from the cell during the test period. This loss of lithium is tentatively attributed to its

migration through an electrolyte film on the tantalum crucible to the Vycor crucible and its subsequent reaction with the Vycor to form a product that is not detectable by the acid-base titration.

TABLE VI. Distribution of Lithium After Operation of Li/LiCl-KCl/Li(Al) Cell

Cell Component	Lithium Found		Percent of Initial Lithium
	g	A-hr	
Steel wool electrode	0.026	0.10	3.3
Lithium-aluminum electrode	0.139	0.54	17.1
LiCl-KCl electrolyte	0.341	1.32	42.1
BeO cup	0.037	0.14	4.6
Vycor crucible[a]	0.081	0.31	9.9
Total	0.624	2.41	77.0

[a]The Vycor crucible was severely attacked by the lithium.

During Discharge 24, the cell was completely discharged. The discharge capacity of the cell, 1.89 A-hr, was very likely limited by the quantity of lithium available (see Table VI), rather than by the effect of the water that was added to the cell. It is suspected, however, that this complete discharge removed all of the lithium from the steel-wool support material, thereby making the active sites more susceptible to reaction with the water and other impurities present in the cell. The rapid loss of lithium from the electrode, after Discharge 24, suggests that the presence of water in the salt at the ∿150 ppm level causes a significant loss in the lithium-retention properties of the steel wool if the lithium electrode is discharged completely. The loss of lithium from the cell prior to Discharge 24 probably resulted from the reaction of the lithium with the Vycor crucible, rather than from a deterioration of the lithium-retention characteristics of the steel wool.

3. Post-Test Examination of Lithium Electrodes

Two lithium electrodes from lithium/sulfur cells that had been operated previously in the cell development work were examined to gain a better understanding of the chemical phenomena associated with lithium retention. The two electrodes, which employed nickel Feltmetal as the support material, had been used in Cell WS-2, a Li/S-15 at. % As cell; the electrical performance tests of this cell have been reported previously.[7] Electrode A, the first lithium electrode used in the cell, had exhibited poor lithium retention, whereas Electrode B, the second electrode used in the cell, had exhibited good lithium retention.

Ion-probe analyses were performed in Electrode A and on the as-received nickel Feltmetal to determine whether a correlation could be established between the chemical composition of the lithium electrode and its lithium-retention characteristics. The results indicated that Electrode A contained sulfur and silicon, which were not present in the as-received Feltmetal. The presence of sulfur probably resulted from the transfer of some sulfur from the sulfur

electrode to the lithium electrode. The presence of silicon is attributed to the use of quartz wool in the upper portion of the furnace well to inhibit convection of the helium atmosphere over the cell.

Electrodes A and B were then analyzed chemically for sulfur and lithium metal. Sulfur was determined as sulfide by a gas-chromatographic procedure, and lithium metal was determined by a simple acid-base titration. Electrode A contained no lithium metal and 1 wt % sulfur, whereas Electrode B contained 5.2 wt % lithium and <20 ppm sulfur (the limit of detection of the method). These results indicate that the presence of sulfur in the lithium electrode results in poor lithium retention.

B. Solubility of Lithium in Molten LiCl-KCl Electrolyte

(B.S. Tani, D. R. Vissers, and J. R. Birk*)

The presence of dissolved lithium in the LiCl-KCl eutectic electrolyte of a lithium/sulfur cell may play an important role in the operating characteristics of the cell. A high lithium solubility (*e.g.*, 1 mol %) would tend to result in rapid self-discharge of the cell by diffusion of the lithium from the negative (lithium) electrode to the positive (sulfur) electrode. Even low levels of dissolved lithium (<0.1 mol %) could affect the electronic conduction of the electrolyte, as well as its corrosive properties.

Although no data are available on the solubility of lithium in the LiCl-KCl eutectic at the cell operating temperature of 400°C, Smirnov and Podlesnyak[8] have reported solubility data in the range from 600 to 800°C. Extrapolation of these data gives a value of 0.13 mol % for the solubility of lithium in LiCl-KCl at 400°C.

This solubility value was used to estimate the rate of self-discharge of a lithium/sulfur cell by the normal diffusion of lithium through the electrolyte to the sulfur electrode. The rate of lithium transport was calculated from Fick's law:

$$F = \frac{D\ (\Delta C)}{\ell}$$

where F is the flux (mol cm^{-2} sec^{-1}), D is the diffusion coefficient (assumed to be 10^{-5} cm^2 sec^{-1}), ℓ is the interelectrode distance (assumed to be 0.5 cm), and ΔC is the difference between the concentration of lithium in the electrolyte at the surface of the lithium electrode (4×10^{-5} mol cm^{-3} at 400°C and that at the surface of the sulfur electrode (zero). The calculated flux is 8×10^{-10} mol cm^{-2} sec^{-1}. For an electrode containing 0.5 A-hr (0.13 g) of lithium per square centimeter, 270 days would be required for complete discharge by diffusion of lithium metal to the sulfur electrode.

In actual practice, it appears that self-discharge occurs in a much shorter period of time. For example, complete discharge of a cell, in which no measurable sulfur loss was observed, occurred in about 10 days.[9] Thus, the diffusion of elemental lithium does not appear to be the predominant mechanism of self-discharge. Other mechanisms which may be important are (1) convective trans-

---

*Industrial Participant, Atomics International Division of Rockwell International.

port of elemental lithium, (2) transport of sulfur-bearing species through the electrolyte to the lithium electrode, and (3) electronic conduction by the molten salt (which might be enhanced by the presence of dissolved lithium, as discussed earlier).

Plans are currently being made to investigate the electronic conduction of molten LiCl-KCl eutectic saturated with lithium.

C. Solid-Electrolyte Studies

(B. S. Tani and D. R. Vissers)

The use of a solid electrolyte capable of lithium-ion conduction would have the potential advantages in lithium/sulfur cells of low self-discharge rates and reduction or elimination of sulfur losses, since the sulfur compartment could be hermetically sealed and sulfur could not migrate through the solid barrier. However, the ionic conductivities of most solid electrolytes are much lower (by a factor of $\sim 10^3$) than those of molten salts. Nevertheless, a small experimental effort to seek a solid electrolyte having sufficient lithium-ion conductivity for use in lithium/sulfur cells appeared to be warranted.

Ceramic electrolytes such as "beta alumina" ($Na_2O \cdot 11Al_2O_3$) are being developed for use in sodium/sulfur batteries. The conductivity of beta alumina is reported to be about 0.2 $ohm^{-1} cm^{-1}$ above 300°C.[10] It is possible to substitute lithium ions for sodium ions in beta alumina by a two-step ion-exchange procedure in which the sodium ions are first replaced by silver ions and the silver ions are subsequently replaced by lithium ions.[11,12]

An attempt was made to convert beta alumina to the lithium-ion form by a modified procedure involving substitution of silver ions for sodium ions by ion exchange, followed by electrochemical replacement of the silver ions by lithium ions. The starting material was a beta-alumina tube* having an outside diameter of 0.9 cm, a wall thickness of $\sim$0.1 cm, and a length of 11.43 cm. The exchange of sodium ions with silver ions was completed by placing the beta-alumina tube overnight in molten $AgNO_3$ at 252°C. On the basis of the original formula, $Na_2O \cdot 11Al_2O_3$, and the weight gain of the tube, the replacement of sodium ions by silver ions was complete.

A cell of the type $Li(Al)/LiF\text{-}LiCl\text{-}LiI/Ag_2O \cdot 11Al_2O_3/LiF\text{-}LiCl\text{-}LiI/Ag$ was constructed for the exchange of lithium ions for silver ions in the silver beta alumina. The molten-salt electrolyte in this cell was the 11.7 mol % LiF-29.1 mol % LiCl-59.2 mol % LiI eutectic (mp, 341°C). The tantalum cell housing was fabricated with the lithium-aluminum alloy located on the bottom and the inside wall. This alloy was prepared by charging the lithium electrochemically into aluminum fibers, which were contained in a tantalum sheath.

The cell was heated slowly (1°C/min) to 373°C. When additional solid LiF-LiCl-LiI electrolyte was added to maintain the liquid level at the proper height, the silver beta-alumina tube fractured at the liquid-electrolyte level. When the tube was removed from the cell, it was found to be cracked throughout and there was a black coating on its surface.

---

*Fabricated by the Toshiba Electric Co., Japan.

The results of this study suggest that the beta-alumina tube was chemically attacked in this system. A silver electrode potential of 0.2 V relative to the lithium-aluminum electrode suggests that free lithium may have been present in the cell, which could have resulted in attack of the beta alumina. Further attempts to prepare the lithium form of beta alumina by this method would require detailed investigations of the electrochemical procedure for replacing silver ions by lithium ions. No additional work on solid electrolytes for lithium/sulfur cells is anticipated in the near future.

IV. MATERIALS TESTING AND FABRICATION
(J. E. Battles)

The fabrication of various cell components, such as electrical feedthroughs, insulators, electrode separators, current collectors, and cell housings requires a variety of metallic and ceramic materials. These materials must be resistant to corrosive attack by various combinations of lithium, LiCl-KCl electrolyte, and sulfur (plus additives which make up the positive-electrode environment). In general, the use of oxide ceramic materials as electrical insulators is limited to those oxides that are thermodynamically more stable than lithium oxide (Li_2O), such as BeO, ThO_2, Y_2O_3, MgO and $MgAl_2O_4$. For metallic materials, the most severe condition exists when the metal is at the sulfur-electrode potential. These conditions often result in a rapid electrochemical attack on most metals, depending on the cell charge voltage.

Since the cell housings or containers will most likely be metallic, an electrical feedthrough with an insulator is required for isolating at least one electrode from the cell housing. The design and development of a reliable, low-cost electrical feedthrough for sealed cells continues to be the major effort of this task.

A. Feedthrough Development
(K. M. Myles and J. W. Downey)

The development of electrical feedthroughs is complicated by the corrosiveness of the cell environment, which severely limits the number of materials (both metallic and ceramic) that may be used for fabrication and by the need to develop ceramic-to-metal techniques for corrosion-resistant hermetic seals. Although a number of feedthrough designs are being contemplated for use in Li/S cells under development for vehicular propulsion applications, a logical preferred choice from the standpoint of weight, size, cost and durability is a ceramic-to-metal seal assembly.

Preliminary corrosion and compatibility tests had indicated that $CaZrO_3$ and E-Brite 26-1 stainless steel* were reasonable starting materials for the development of such a feedthrough. Also, the coefficients of thermal expansion appeared to be reasonably well matched. Subsequent in-cell and planned-interval corrosion tests (see Section IV.C, below) have tended to detract from the initial optimism with regard to $CaZrO_3$.

A schematic representation of the present feedthrough design is shown in Fig. 16. The conductor is brazed directly to the $CaZrO_3$ insulator, which in turn is brazed to the E-Brite housing using an active metal braze. For ease in fabrication, the E-Brite housing is made in two parts, namely, a tube which surrounds the $CaZrO_3$ insulator and the flat lid of the cell; these are mechanically pressed initially and later metallurgically bonded together. The thickness of the E-Brite is about 0.5 mm, the diameter of the $CaZrO_3$ body is about 9.5 mm, and the diameter of the conductor is about 3.2 mm.

---

* A ferritic stainless steel developed by Airco Vacuum Metals of the Air Reduction Co., Inc.; composition (wt %): Fe-26 Cr-1 Mo.

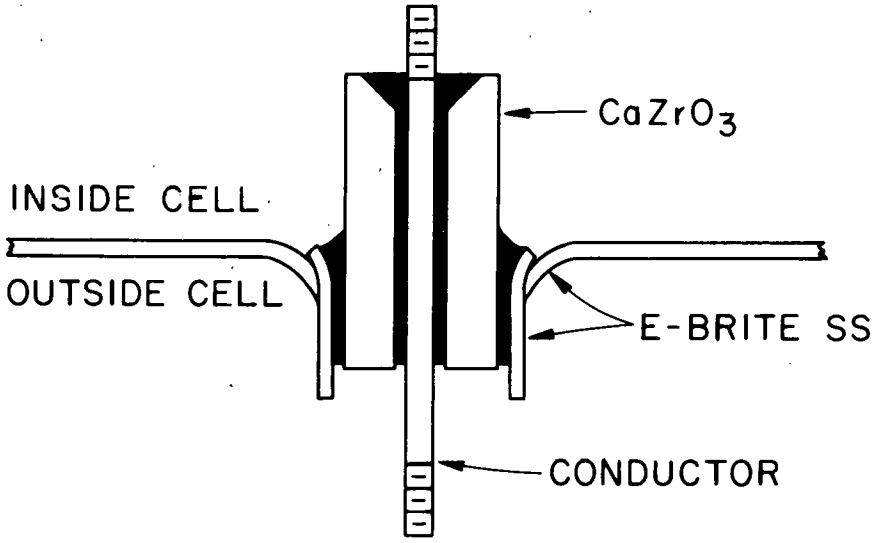

Fig. 16. Schematic Representation of Brazed-Type Electrical Feedthrough

Several factors that severely limit the selection of a bonding agent are the corrosiveness of the cell environment; the operating temperature of the cell; the mutual wettability of the E-Brite, $CaZrO_3$, and conductor by the bonding agent; and the compatibility of the respective coefficients of thermal expansion. Secondary factors include the mechanical strength of the bond; the effect of air on the bond; and the cost, availability, and toxicity of the bonding agent. Consideration of these factors suggested the testing of an active metal brazing alloy of the composition Zr-8 wt % Ni-8 wt % Cr, which had been previously developed at Argonne National Laboratory.[13] This alloy had the tendency to cause excessive dissolution of the stainless steel when superheated sufficiently for reasonable fluidity. Additional alloy compositions were evaluated: Zr-16 wt% Fe cracked upon cooling; Zr-8 wt % Fe was porous; Zr-6 wt % Cr-6 wt % Fe-6 wt % Ni yielded good results but has an excessively high liquidus temperature due to the presence of a primary phase. With the aid of the electron microprobe analyzer, the eutectic composition was determined as Zr-2 wt% Cr-6 wt % Fe-6 wt % Ni (mp, $\sim 955 \pm 5°C$) and it is this alloy that has been used to braze the feedthrough components. The alloy is prepared by arc-melting prescribed quantities of high-purity Zr, Fe, Ni, and Cr in a helium atmosphere, followed by levitation melting to assure complete homogeneity and minimize contamination. Dilatometric measurements are being conducted to determine the coefficient of thermal expansion for this alloy.

Although the direct brazing of metals to ceramics is very difficult without an intermediate metallizing operation, preliminary tests results have indicated that such a process is practical for the materials involved in the present feedthrough. Direct metal-to-ceramic brazing is highly desirable because of its simplicity, lower cost, and the corrosion resistance of the braze.

An analysis of the thermal stresses produced in the ceramic body upon cooling from the brazing temperature indicated that, with the configuration shown in Fig. 16, the ceramic would be put into compression by the feedthrough

sleeve and, thus, not be susceptible to cracking upon cooling from the brazing temperature. Furthermore, since the thermal expansion coefficients for E-Brite and $CaZrO_3$ were reasonably close (*i.e.*, $\alpha = 13.7 \times 10^{-6}/°C$ and $\alpha = 10.0 \times 10^{-6}/°C$, respectively), the initial tests were made with E-Brite electrodes. Ultimately, molybdenum or tungsten may be more likely choices for electrode materials; unfortunately, these metals have lower coefficients of thermal expansion ($\sim 5 \times 10^{-6}/°C$) that are very poorly matched to that of $CaZrO_3$ and would be expected to produce tensile stresses in the ceramic that might result in both radial and cross-sectional cracking.

Several alternatives to alleviate this potential difficulty in sealing the electrode to the ceramic are under evaluation. One is to use a solder glass as the sealant material and another is to redesign the feedthrough configuration, as shown schematically in Fig. 17, to accomodate better the thermal expansion differences of the feedthrough components throughout the brazing cycle.

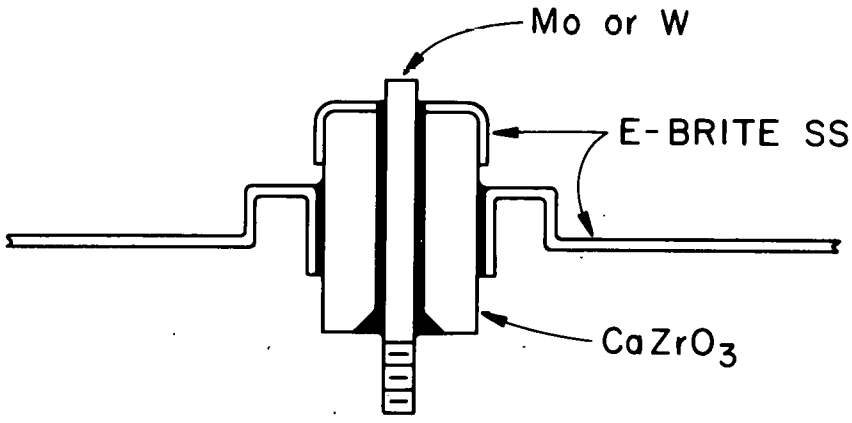

Fig. 17. Schematic Representation of Brazed-Type Feedthrough for Materials of Construction with Different Coefficients of Thermal Expansion

To facilitate the brazing operation, a brazing jig was fabricated that properly positioned the various elements of the feedthrough during brazing and also controlled the heat dissipation throughout the brazing cycle. In addition, the jig acted as a black body for accurate determinations of the temperature of the feedthrough. In brief, the steps in brazing the feedthrough include degassing under vacuum at 900°C to prevent oxidation of the active metal braze compound, brazing at 1025°C (melting temperature of braze compound, 955-960°C), and a cool-down that is slow enough to avoid thermal cracking, yet fast enough for production purposes.

A cross section of the completed feedthrough was examined metallographically, and a macrograph is shown in Fig. 18. The ceramic shown was isostatically pressed and, as a result, exhibits a rather high degree of porosity (density, about 90% of theoretical). Excellent metallurgical bonding was obtained between the E-Brite, the braze alloy, and the ceramic; the latter is seen better in Fig. 19. In the particular feedthrough shown, the braze flowed

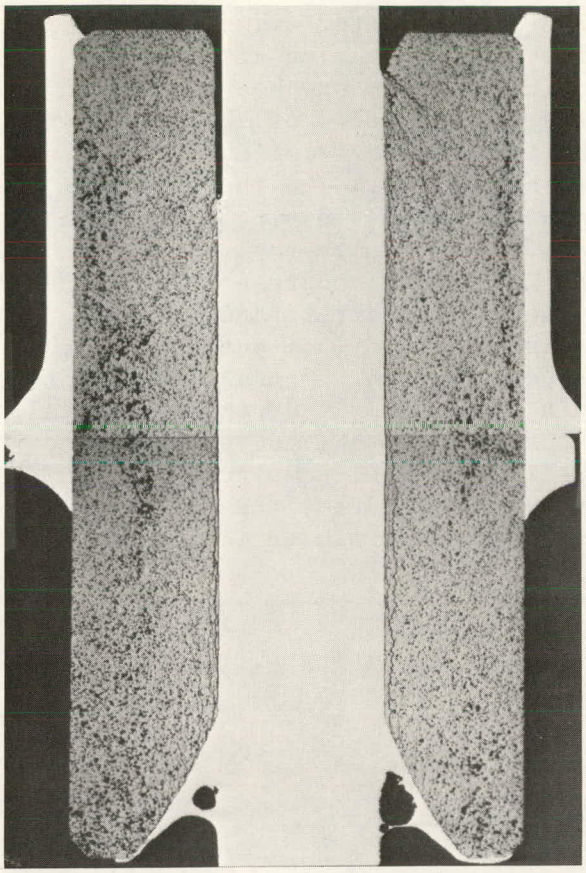

Fig. 18.

Photomacrograph of Cross Section of Brazed Feedthrough (Note bonding of feedthrough sleeve to $CaZrO_3$ insulator and small cracks in the insulator adjacent to the conductor (As-polished, 5.5X). ANL Neg. No. 308-3451

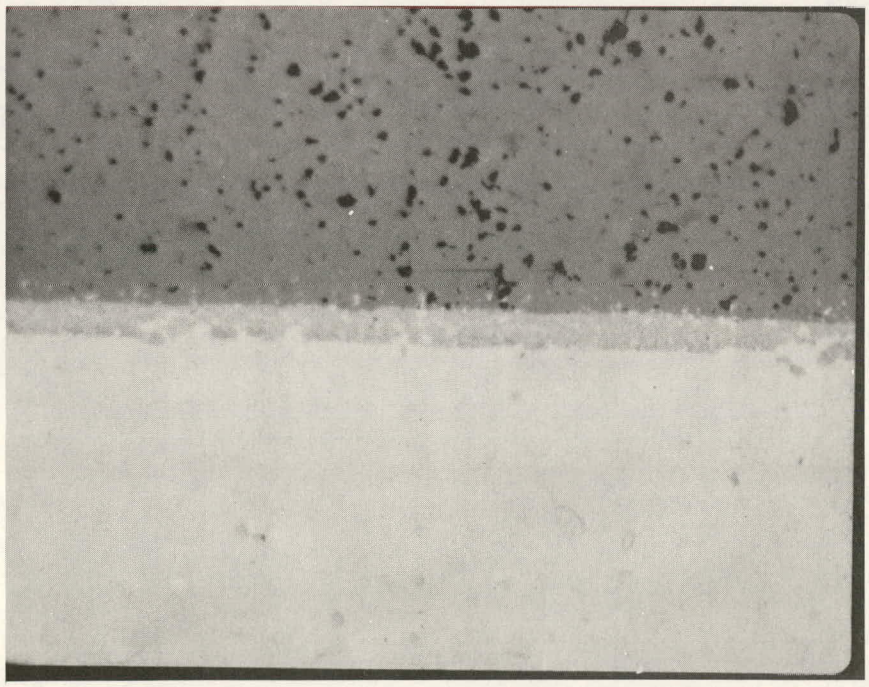

Fig. 19. Photomicrograph Showing Excellent Bonding of Braze Metal to $CaZrO_3$ Insulator (As-polished, 400X). ANL Neg. No. 308-3407

completely down the annulus between the E-Brite conductor and the $CaZrO_3$ insulator. A major difficulty encountered with initial brazing attempts was a lack of braze-metal flow along the conductor. This problem has been corrected by increasing the braze temperature to increase the fluidity of the braze metal and by adding heat sinks to alter the heat-flow characteristics in the feedthrough during the brazing operation. As shown in Fig. 18, there is some evidence that the conductor and the ceramic separated, leaving a hairline crack. This, presumably, is due to the differences in thermal expansion between the two materials. Furthermore, the isostatically pressed-and-sintered $CaZrO_3$ bodies appear to be grainy and to lack strong intergranular bonds. A similar completed feedthrough with a pressure-sintered (hot-pressed) $CaZrO_3$ insulator is shown in Fig. 20. Here, the porosity and the granular structure are noticeably absent, thus resulting in a significantly stronger material. Unfortunately, a crack pattern developed that now appears to be related to thermal stresses generated within the ceramic upon cool-down from the braze temperature. Efforts are presently under way to eliminate the difficulty by altering the braze cycle to allow for a substantially slower cool-down.

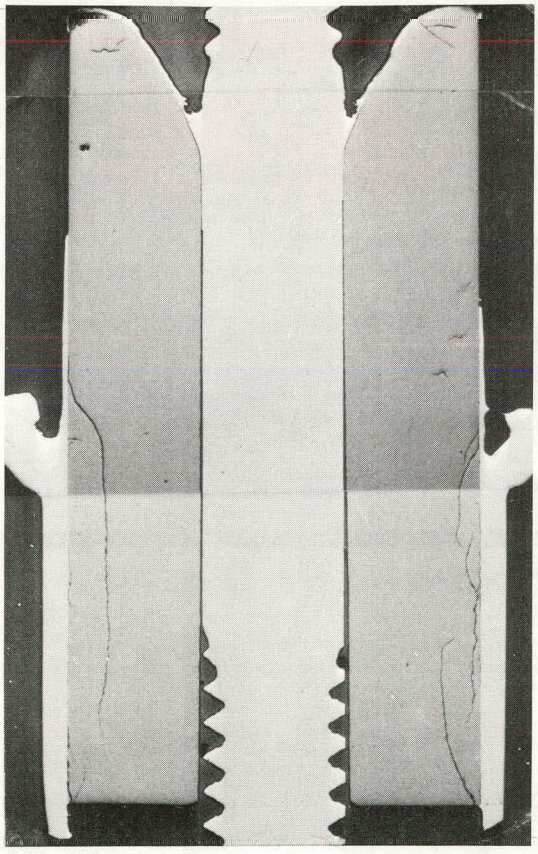

Fig. 20.

Photomacrograph of Cross Section of Brazed Feedthrough Showing Thermal Cracks at Sleeve/Ceramic Interface (As-polished, 5.5X). ANL Neg. No. 308-3408

Somewhat aside from the above discussion but relevant to the feedthrough development, additional braze tests have been conducted to determine the bonding characteristics of this zirconium-base braze metal with other metals. Preliminary results have indicated that satisfactory bonds are obtained with austenitic stainless steels, iron, and molybdenum. However, the braze metal

does not appear to form a well-defined reaction zone with molybdenum, as it does with E-Brite 26-1. Additional tests have been initiated to determine the ability to obtain reasonable bonds between this braze metal and various ceramic materials (*e.g.*, MgO, $MgAl_2O_4$, and AlN).

B. Insulator and Separator Studies
(J. E. Battles and J. L. Settle)

Lithium/sulfur batteries for vehicular propulsion will require ceramic or insulator materials for three specific functions: (1) electrical feedthrough insulators, (2) electrode separators, and (3) cell and battery insulation. Additional needs for insulator materials may arise as cell and battery development progresses. In the case of feedthrough insulators and electrode separators, the selection of materials for potential application is limited to those that will withstand the corrosive environment of the cell. Materials for exterior electrical and thermal insulation are not subject to these limitations, and hence, will be less difficult to provide.

Calcium zirconate was selected for feedthrough insulators and electrode separators for initial development primarily because preliminary lithium-compatibility test results were favorable (ANL-7998, p. 73) and because $CaZrO_3$ was readily brazed to metals using a zirconium-base braze alloy (see Fig. 19). Additional tests have been conducted which indicated that the $CaZrO_3$ material used thus far is not totally compatible with lithium in long-term tests (see Section IV.C).

The procedure for making $CaZrO_3$ insulators has been to mix the $CaZrO_3$ powder with an organic binder (*e.g.*, Carbowax, paraffin, or Mobilcer R*) suspended in an aqueous solution or dissolved in an organic solvent. This slurry is allowed to dry at room temperature, powdered, and then isostatically pressed in a rubber mold of the desired size and shape using pressures of 15,000-25,000 psi. After pressing, the green body is removed from the mold and calcined in an air furnace. The binder is added to obtain sufficient green strength to permit removal of the green body from the mold and subsequent handling. After calcining, the ceramic body is sintered in a vacuum or helium atmosphere at temperatures to about 2000°C. Process variables that influence the properties of the finished ceramic body are (1) particle size of starting powder, (2) amount of binder added (and in some cases, the type of binder), (3) pressure applied during molding, (4) calcining and sintering temperatures, and (5) time at sintering temperature.

The calcium zirconate powder was purchased from Cerac, Inc. and from the Zirconium Company of America (Zircoa). The average particle size of the $CaZrO_3$ powder was about 44 μm for the Cerac material and 5 μm for the Zircoa material. Ceramic bodies fabricated from the as-received Cerac powder reached final densities in the range of 75 to 80% of the theoretical density of 4.78 g/cm^3, whereas final densities in the range of 75 to 90% of theoretical were achieved with the Zircoa powder. The higher densities for both materials were obtained by sintering at about 2000°C; lower sintering temperatures yielded lower densities. Since the preparation and sintering conditions were the same for

*A product of Mobil Oil Co.

both materials, it was evident that a more dense ceramic body was obtained using the material with the smaller particle size.

These results suggested that higher sintered densities could be obtained by starting with a $CaZrO_3$ powder of even smaller particle size. Accordingly, portions of both materials were ball-milled with alumina balls for periods of 2, 4, and 8 days (the average particle size and distribution were not determined). The Zircoa $CaZrO_3$ powder was wet-milled, whereas the Cerac material was dry-milled. By using these materials and varying only the temperatures and times of calcining and sintering, sintered densities of 92 to 94% of theoretical were obtained with the Zircoa material that was ball-milled for 8 days and sintered at about 1900°C. Similarly, the Cerac material which had been ball-milled for 8 days yielded sintered densities of 94 to 98% of theoretical when sintered at about 1700°C. For both materials, specimens sintered at 2000°C were less dense, more porous, and had large grains, thus indicating over-sintering.

The results of these studies indicated that the particle size and sintering temperature are the two most important process parameters affecting the properties of the finished ceramic. Sintering at too high a temperature (over-sintering) leads to a final product which is mechanically weak, pervious, and unsuitable for our application. The process conditions which yielded the best properties were to start with an extremely fine powder with 1-2 wt % organic binder, isostatically press at 15,000 to 25,000 psi, calcine at about 750°C overnight for binder removal, and sinter at about 1700°C for 2 hr. This procedure yielded an essentially impervious ceramic with a small grain structure and with good mechanical properties.

Metallographic examination of sintered specimens prepared from the as-received $CaZrO_3$ powders showed the presence of an impurity phase at the particle boundaries which appeared to have been liquid at the sintering temperatures (1650 to 2000°C); this phase was later found to react with molten lithium. (Investigations to identify this material and attempts to purify the as-received $CaZrO_3$ are described in Section IV.C.2, below.) Because of the problems encountered, efforts are being made to find a commercial source of higher-purity $CaZrO_3$. Also, starting materials have been ordered which will permit us to synthesize high-purity $CaZrO_3$.

A porous electrode separator material, such as a ceramic cloth or a porous ceramic disk, that is resistant to the cell environment would permit closer spacing of the lithium and sulfur electrodes and would help to reduce the overall weight and volume of the cells. For this purpose, commercial vendors were contacted to determine the availability of ceramic cloths. At present, the only available ceramic cloths are BN cloth from the Carborundum Co. and Zircar (stabilized zirconia) cloth from the Union Carbide Corp. Corrosion tests have shown that stabilized zirconia is not compatible with lithium at 400°C; however, this material may be useful in cells having Li-Al electrodes (and a lower lithium activity), which are being developed in the AEC battery program. Boron nitride cloth may be a useful electrode separator for Li/S cells if properly treated to remove the residual boron and B_2O_3. In addition to these cloth materials, Union Carbide Corporation has provided us with small samples of Y_2O_3 cloth, which they prepared on an experimental basis. The results of lithium-compatibility tests with the Y_2O_3 are discussed in the following section.

The fabrication of thin, porous ceramic disks has been initiated. A series of porous $CaZrO_3$ disks has been prepared using powdered $CaZrO_3$ of various mesh sizes and various organic binders; the preparations and results are summarized in Table VII. The volume fractions of porosity of the disks ranged between 21 and 39% and represent a fairly broad range of pore character. Efforts will be continued to develop and characterize porous ceramics for possible use as electrode separators.

TABLE VII. $CaZrO_3$ Pressed at 10,000 psi and Sintered at 1450°C for 60 hr

Starting Material (U.S. mesh size)	Binder	Shrinkage, %	Apparent Porosity, %
-60+200	4.5% Mobilcer R	5	33
-50+60	9.5% Mobilcer C	3	39
-80+100	9% Mobilcer R	4	36
-200	4.5% Mobilcer R	14	21

C. Materials Evaluation

(F. C. Mrazek and J. E. Battles)

Before components such as electrical feedthroughs, insulators, current collectors, and electrode separators can be fabricated for a practical Li/S cell, it is necessary to identify those materials (metallic and ceramic) that show promise of having long-term compatibility with the corrosive cell environment. The performance of these various materials can be evaluated fully only through their use in operating cells and batteries. This type of materials testing, however, is expensive and time-consuming. For this reason, short-term static corrosion tests have been used to identify those materials that are potentially useful for cell application. These corrosion tests are being continued to identify other materials for potential application with emphasis on light-weight, low-cost materials. In addition to the short-term tests, long-term and planned-interval type tests have been initiated to evaluate the compatibility of the more promising materials for long-term cell operation.

1. Evaluation of Metals

Planned-interval corrosion tests[14,15] provide data on the accumulated effects of corrosion at several times under a given set of conditions; these data may be extrapolated to obtain an indication of the long-term corrosion behavior of these materials. These tests also provide information on changes that might occur in corrodibility of the metal or in the corrosiveness of the liquid during the test. The time intervals selected are generally determined by the expected corrosion rate of the material being tested.

Planned-interval corrosion tests in LiF-LiCl-KCl electrolyte have been completed on the following materials: Types 304, 316, 430, and E-Brite 26-1 stainless steels, Armco ingot iron, high-purity iron (99.999%), and

aluminum-clad Type 434 stainless steel. The results are listed in Table VIII. The corrosion rates were calculated from the weight loss, area, and exposure time;these rates are reported in micrometers per year (μm/yr). The values listed are the average of the corrosion rates obtained in each of the four intervals. (The intervals were 200 hr for all materials except E-Brite 26-1, for which the intervals were 400 hr.) The observed corrosion rates for the Type 304, 316, and 430 stainless steels were extremely low (2 μm/yr) and, except for a few shallow pits, the materials appeared unaffected. Although the corrosion rate for E-Brite 26-1 was greater (8 μm/yr), no evidence of pitting was found in the E-Brite 26-1 samples. The observed difference in the corrosion rate for Armco iron (12 μm/yr) and that for high-purity iron (31 μm/yr) is surprising: generally, better corrosion resistance is obtained with elements of higher purity (Armco iron is about 99.9% pure). The aluminum-clad Type 434 stainless steel sample showed a fairly high corrosion rate (130 μm/yr). Visual and metallographic examination showed that the aluminum was selectively corroded while the Type 434 stainless steel was relatively unaffected. Of course, a galvanic couple is established when aluminum is placed in contact with stainless steel in an electrolyte, with aluminum being anodic. The stainless steel test samples were examined metallographically for evidence of intergranular corrosion, which results from selective corrosion along grain boundaries.* No evidence of intergranular corrosion was observed in any of the samples.

TABLE VIII. Results of Planned-Interval Corrosion Tests in LiF-LiCl-KCl Electrolyte at 400°C

Material	Corrosion Rate,[a] μm/yr
Type 304 stainless steel	2
Type 316 stainless steel	2
Type 430 stainless steel	2
E-Brite 26-1 stainless steel	8
Armco ingot iron	12
Iron (99.999% Fe)	31
Al-clad Type 434 stainless steel	130

[a] Each corrosion rate given represents an average of the measured corrosion rates from each of the four intervals. The time intervals for each material were 200 hr except for E-Brite 26-1 (400 hr).

The measured corrosion rates for each interval were relatively constant for a given sample material, thus indicating that the metal corrodibility and liquid corrosiveness did not significantly change during the test. Any changes in either of these properties would have been indicated by significant

* A prerequisite for intergranular corrosion is that the stainless steel be sensitized, *i.e.*, chromium carbides ($Cr_{23}C_6$) are precipitated at the grain boundaries. This condition is caused by heating of the stainless steel (such as Type 304) in the temperature range of 450-850°C or slow cooling through this temperature range from a higher temperature, as might occur in welding.

increases or decreases in the corrosion rates for each interval.

2. Evaluation of Ceramics

The initial compatibility tests of sintered $CaZrO_3$ in lithium at 400°C indicated a significant penetration of lithium into the porous sample (Fig. 36, p. 77, ANL-7998). At that time, it was believed that penetration was due to the rather porous structure of the $CaZrO_3$ (<90% of theoretical density). However, additional metallographical examinations of sintered samples of $CaZrO_3$ (see Section IV.B) showed the presence of a minor phase in the particle boundaries (see Fig. 21) which appears to have been liquid at the sintering temperatures (1600 to 2000°C).

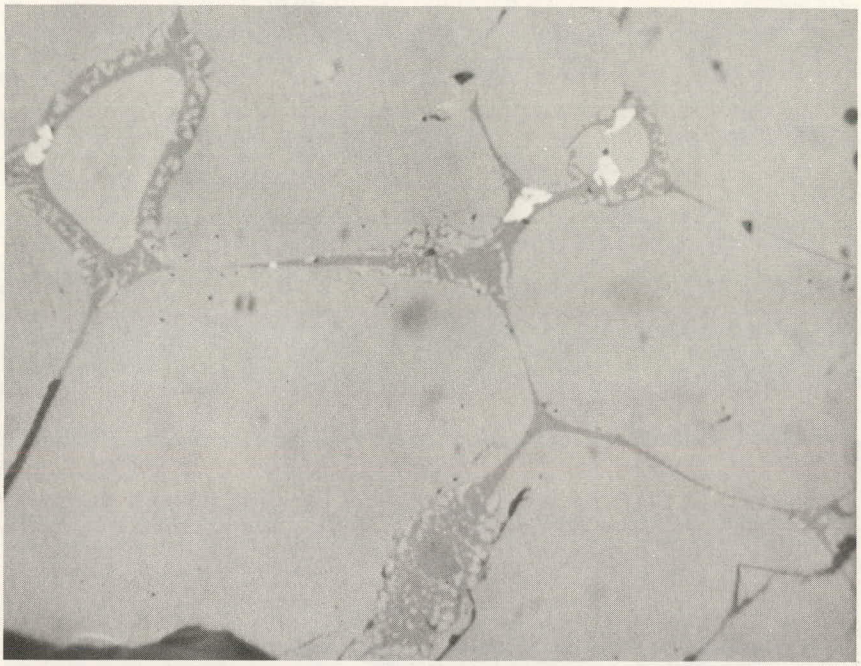

Fig. 21. Photomicrograph of As-Sintered $CaZrO_3$ Showing a Low-Melting Impurity Phase at Particle Boundaries. (As-polished; 480X)

Samples were prepared for examination by oil polishing. Subsequent tests showed that this minor phase was water-soluble and, hence, was not detected earlier because water was used in the normal polishing procedure. Chemical analysis indicated that the as-received Zircoa $CaZrO_3$ contains 0.5 wt % SiO_2. Also, the material contains some unreacted CaO and ZrO_2. Electron microprobe analysis of sintered specimens showed that the minor phase contained, primarily, calcium and silicon with a small amount of aluminum and zirconium. These results indicate that the minor phase is probably a calcium silicate ($CaSiO_3$) which is soluble in water and also reacts with molten lithium. For removal of the silica and calcia, the as-received $CaZrO_3$ powder was acid-leached (in 0.1*N* or 1*N* HCl) and thoroughly rinsed with distilled water. Metallographic examination of sintered specimens indicated that the leach treatment

did effectively remove the silicate phase. However, the treatment yielded a product containing excess cubic zirconia (solid solution of ZrO_2 and CaO) which appeared as discrete particles in a matrix of $CaZrO_3$. Compatibility tests in lithium have shown that cubic zirconia will react with lithium and, hence, is undesirable for our purposes.

Conflicting results have been obtained with the compatibility tests of sintered $CaZrO_3$ in lithium at 400°C. The initial tests (200-hr exposures) showed only a slight discoloration and no change in the resistivity of the $CaZrO_3$. However, subsequent tests have indicated considerable discoloration and the presence of a conductive surface layer. The latter is shown in Fig. 22. This $CaZrO_3$ sample was exposed to lithium at 400°C for 600 hr (Run BM-17-A). Although the surface layer appears metallic, X-ray diffraction analysis of material scraped from the surface showed only $CaZrO_3$ (a very minor phase would not be detected by X-ray diffraction).

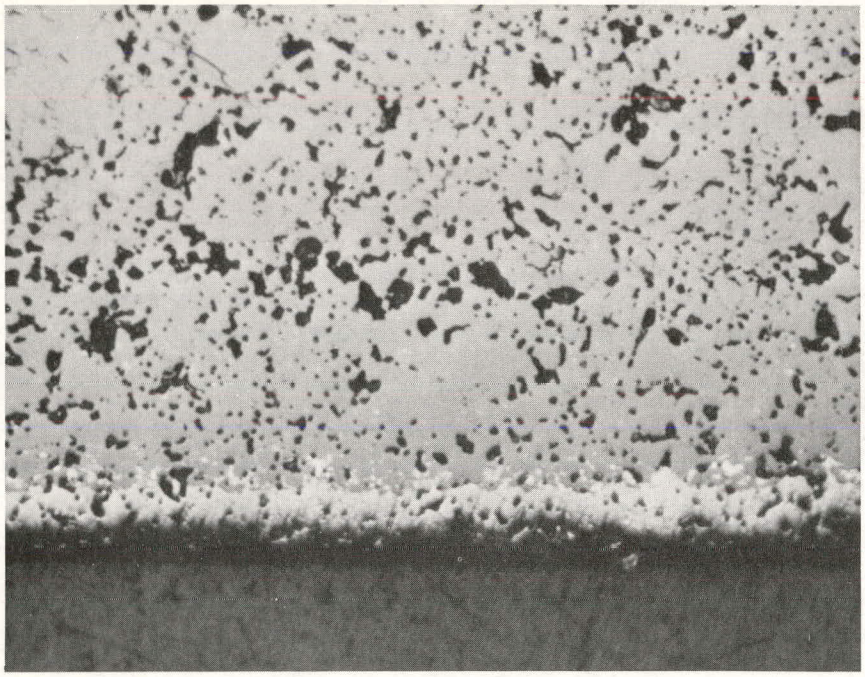

Fig. 22. Photomicrograph Showing Conductive Layer Formed on Surface of $CaZrO_3$ Exposed to Lithium at 400°C for 600 hr [The conductive layer (bottom of figure) appears metallic. As-polished, 300X]

Oxygen analysis of the lithium used in the two compatibility tests indicated that the conflicting results might be related to the quantity of oxygen present in the lithium.* To confirm this suspicion, duplicate samples of $CaZrO_3$ were exposed at 400°C for 400 hr to lithium containing 0.2 wt % and 2 wt % oxygen. Examination showed that the $CaZrO_3$ sample exposed to lithium containing 2 wt % oxygen was discolored and nonconductive, whereas the sample

*The lithium used in the initial tests contained about 2 wt % oxygen, whereas in the second test, the lithium contained about 0.2 wt % oxygen.

exposed to lithium containing 0.2 wt % oxygen was conductive on one surface in addition to being discolored. Photomicrographs of representative areas are shown in Fig. 23. The light colored surface layer shown in Fig. 23a is conductive and, as shown in this photomicrograph, the conductive layer did not cover the entire surface of the sample. No evidence of a conductive surface layer was found on the other sample (Fig. 23b). Additional tests are being conducted to characterize this behavior more fully.

As noted in Section IV.B, a porous ceramic cloth or paper which is resistant to the cell environment is desirable for electrode separators, since this would permit closer spacing of the electrodes and reductions in cell weight and volume. Test samples of Y_2O_3 cloth (satin weave) have been received from Union Carbide Corp. and tested for compatibility with lithium. The test samples were heated in lithium ($\sim$0.2 wt % oxygen) at 400°C for periods of 200, 400, 600 and 1000 hr. The adhering lithium was removed from each sample by dissolution in methanol. All samples showed small areas of slight discoloration, but there was no apparent change in the resistivity of the material. Metallographic comparison of the as-received and tested material indicated no change in appearance. However, the material did appear to be more fragile after testing in lithium.

Because of the favorable results obtained in these tests, additional material (Y_2O_3 cloth) has been ordered in sufficient quantity to permit testing in operating cells.

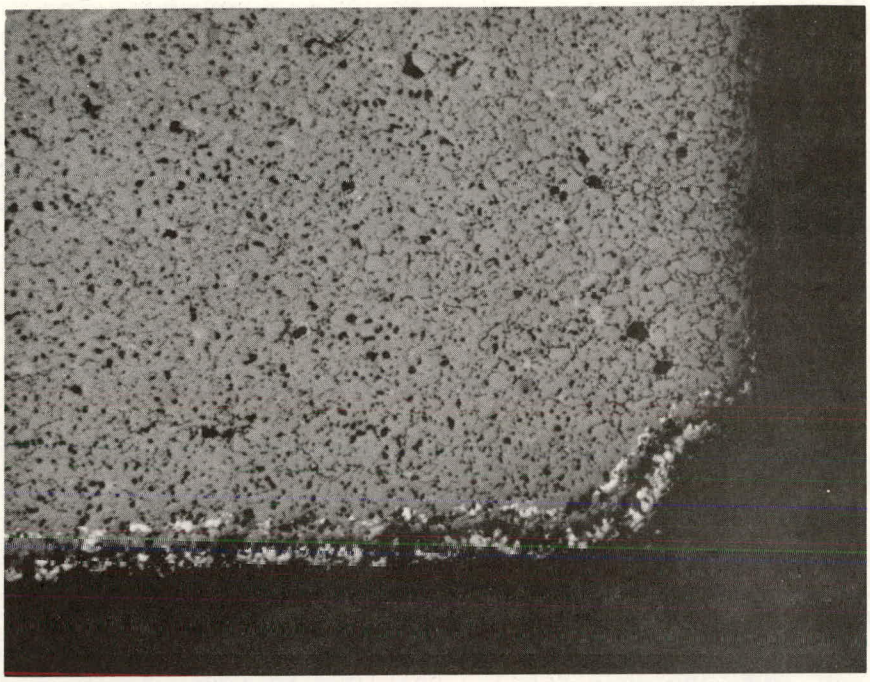

a.

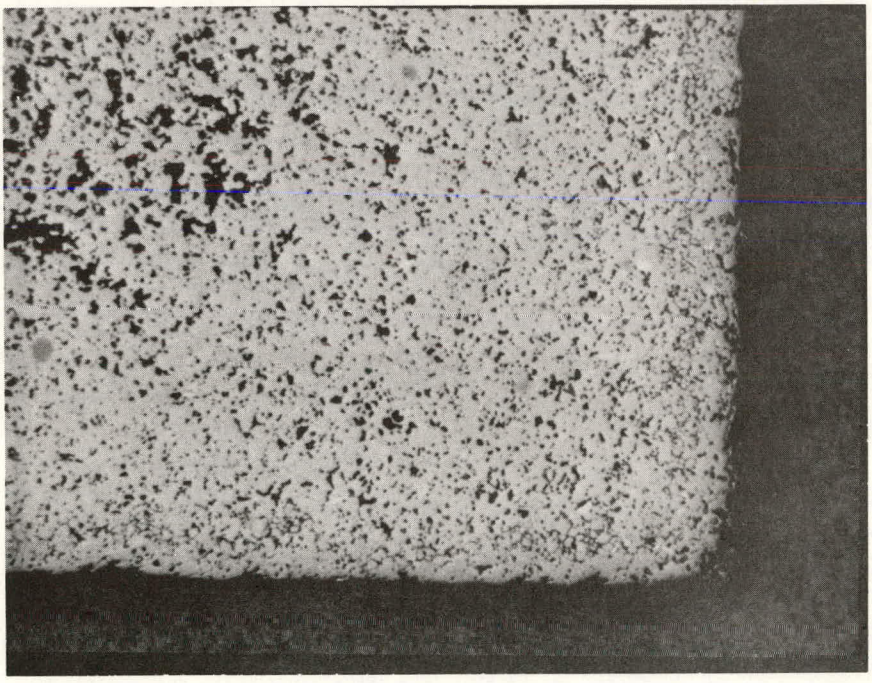

b.

Fig. 23. $CaZrO_3$ Exposed to Lithium at 400°C for 400 hr
a. Oxygen Content of Lithium, 0.2 wt % (200X)
b. Oxygen Content of Lithium, 2 wt % (200X)

REFERENCES

1. E. J. Cairns, E. C. Gay, R. K. Steunenberg, H. Shimotake, J. R. Selman, T. L. Wilson, and D. S. Webster, *Development of High-Specific-Energy Batteries for Electric Vehicles, Progress Report for the Period February 1972-July 1972*, ANL-7953, Argonne National Laboratory (1972).

2. E. J. Cairns, P. A. Nelson, E. C. Gay, R. K. Steunenberg, W. J. Walsh, J. E. Battles, H. Shimotake, J. P. Ackerman, M. L. Kyle, and D. S. Webster, *Development of High-Specific-Energy Batteries for Electric Vehicles, Progress Report for the Period August 1972-January 1973*, ANL-7998, Argonne National Laboratory (1973).

3. W. J. Walsh, E. C. Gay, J. D. Arntzen, J. E. Kincinas, E. J. Cairns, and D. S. Webster, *Lithium/Chalcogen Secondary Cells for Components in Electric Vehicular Propulsion Generating Systems, Interim Technical Summary Report No. 5 for the Period May 23, 1971-November 22, 1971*, ANL-7999, Argonne National Laboratory (1973).

4. H. Rawson, *Inorganic Glass-Forming Systems*, p.267, Academic Press (1967).

5. P. A. Nelson, W. J. Walsh, R. K. Steunenberg, J. E. Battles, M. L. Kyle, K. M. Myles, H. Shimotake, N. P. Yao, J. R. Birk, W. D. Tuohig, D. S. Webster and L. Burris, *High Performance Batteries for Off-Peak Energy Storage, Progress Report for the Period January-June 1973*, ANL-8038, Argonne National Laboratory (in press).

6. N. P. Yao, L. A. Heredy, and R. C. Saunders, J. Electrochem. Soc. *118*, 1039 (1971).

7. Ref. 2, p. 38.

8. M. V. Smirnov and N. P. Podlesnyak, Zhur. Priklad. Khim. *43*, 1463 (1970).

9. L. A. Heredy, Atomics International, Canoga Park, California, private communication (1973).

10. J. H. Kennedy and A. F. Sammells, J. Electrochem. Soc. *119*, 1609 (1972).

11. Y. F. Yao and J. T. Kummer, J. Inorg. Nucl. Chem. *29*, 2543 (1967).

12. B. Cleaver, University of Southampton, England, private communication to L. E. Trevorrow (1971).

13. F. D. McCuaig and R. D. Misch, U. S. Patent 2,432,887, assigned to ANL.

14. A. Wachter and R. S. Treseder, Chem. Eng. Progr. *43*, 315 (1947).

15. Ref. 2, p.74.